3
Synthesis and Characterization of Heterogeneous Catalysts

3.1 INTRODUCTION

Heterogeneous catalysis plays an important role in a biological, chemical and pharmaceutical industry. Almost 90% of all chemical reactions involve heterogeneous catalysts in catalytic processes. Industrial heterogeneous catalysts consist of metals or metal compounds supported on an appropriate support. Catalyst supports are to assist effective dispersal of an expensive active catalyst. However, in most cases, the support can contribute to the catalytic activity by modifying or reacting with the other catalytic components. The catalyst support material has been of huge interest because it provides a high surface for stable dispersion of metal nanoparticles, increases the optimal performance of the catalyst, and decreases the amount of costly metal being utilized, which accordingly decreases the total catalyst expense [Bagheri *et al,* 2014, Lam and Luong 2014].

3.1.1 Background of Metal Loaded Carbon Materials

Traditionally, alumina [Weng and Zaera 2014], silica [Toukoniitty and Murzin 2004], titanium [Bagheri and Muhd Julkapli *et al,* 2014], zeolites [Gamez and Köhler *et al,* 1998] and clay [Fraile *et al,* 1998] are often used as supporting materials [Elezovic *et al,* 2016]. Although a number of drawbacks, such as lower electronic conductivity, higher solubility in acidic medium, low thermal stability and a comparatively low surface area, still exist for these supports [Wang *et al,* 2011]. On the other hand, carbon materials are known for being excellent supports [Serp 2009, Groves *et al,* 2012, Li *et al,* 2013, Zhang *et al,* 2013, Guan *et al,* 2014, Melchionna *et al,* 2015], due to their unique properties, like high surface area, chemical inertness, porosity, high thermal and electric conductivity. These characteristic features are very valuable for catalytic process and are not attainable by any other support [Jüntgen 1986, Rodríguez-Reinoso 1998, Hutchings 1999]. The surface of carbon materials needs to be made hydrophilic by functionalisation [Tsang *et al,* 1994, Baughman *et al,* 2002, Carvalho Padilha *et al,* 2016, Wang *et al,* 2016]. Functional groups (-COOH, -OH, -C=O) are generated by treating carbon materials with oxidizing reagents like nitric acid, sulfuric acid and other oxidizing agents. Carbon has many allotropes like graphene, fullerene, carbon nanotubes, carbon fibers, activated carbon and diamond. Out of these, MWCNTs, carbon fibers (CF), activated carbon (AC) and graphene are some of the key nominees as support due to their commercial availability and ease of chemical modification.

Two important steps are used for catalyst preparation.

(a) Activation of carbon materials

(b) Adhesion of metal nanoparticles

(a) Activation of Carbon Materials

Generally, carbon materials are chemically inert and hydrophobic in nature [Fard *et al,* 2016]. Therefore, the carbon materials need to be activated by surface functionalisation. Then functional groups are generated on the surface of carbon to bind the catalyst. Several activation methods are known for functionalisation, to improve the porosity and surface area of carbon nanomaterials [Alegre *et al,* 2014]. The agglomeration of NPs is one of the reasons to use supporting materials. Thus, the strong attachment of NPs is required on the surface of the support [Islam *et al,* 2014].

(b) Adhesion of Metal Nanoparticles

The catalytic processes mainly depend upon the size of nanoparticles, shape and composition, which strongly depends upon preparation methodology and experimental condition (temperature, pH and precursor). Several methods have been used for preparing metal loaded carbon materials, like the wet impregnation method [Derbyshire *et al,* 1986, Dujardin *et al,* 1994, Tsang and Chen *et al,* 1994], the colloidal method [Wilde 2009], ion-exchange, micro-emulsion [Escudero *et al,* 2002], core-shell [Chen *et al,* 2015], hollow spheres [Dong *et al,* 2012] and organic solution approach. Out of the various methods, wet impregnation [Dujardin and Ebbesen *et al,* 1994] is widely used due to the uniform reduction of the metal [Wilde 2009]. In this method, metal and metal salt (metal chloride, nitrate and acetate) precursors are mixed with carbon materials in an organic and aqueous solvent (water, ethanol, acetone and toluene) to form a homogenous mixture, using sonication followed by stirring. The mixture is separated by centrifuge and calcinated under nitrogen gas. Metal is reduced by a different method such as chemical reduction, hydrogen bubbling [Chen *et al,* 2015] or air reduction. In case of chemical reduction, reducing agents such as $NaBH_4$ [López-Suárez *et al,* 2014], sodium formate [Chen and Guan *et al,* 2011], ethylene glycol [Kim *et al,* 2006] and formaldehyde [Chen and Rui *et al,* 2015] have been used.

3.1.2 Background of Synthesis of Control Size and Shaped Metal Nanocrystals

The properties and behavior of metal nanocrystals, in a given catalytic reaction, are subjected to exposed facets. There are selective reports where chemical reagents (CTAB, TOAB and PVP) are used to control the shape and growth of certain facets [Susut *et al,* 2008]. Various agents (stabilizers) are indispensable for controlling the shape of NCs [Yang *et al,* 2008, Zeng *et al,* 2011]. Some of these reagents are readily removed by washing or heating at high temperatures, while some others are quite difficult to remove. It has been reported that these stabilizers can stabilize nanocrystals by two processes; one is electrostatic stabilization and second is steric stabilization [Semagina and Kiwi-Minsker 2009]. In electrostatic stabilization, ions absorb on the surface of electrophilic metal surface and create a coulombic repulsion between electric double layers. In steric stabilization, stabilizer (surfactant and polymers) surrounds the metal centre by the layer of bulky groups and controls the growth of crystallographic orientations using material gap. For example, PVP and polyacrylate have been used as stabilizers for the synthesis of shaped Pt nanocrystals [Teranishi *et al,* 2000, Song *et al,* 2006]. There are many structure-sensitive catalytic reactions [Pradier *et al,* 1994, Studer and Burkhardt *et al,* 2000, Li *et al,* 2002, Arenz *et al,* 2005, Sen and Gökagaç 2007] in which shape and size of nanocrystals affect the catalyst activity [Borodziński 2001, Narayanan and El-Sayed 2005]. Among these studies, noble metal NCs have attracted great attention owing to their fascinating properties and especially their excellent catalytic performance. Sun and co-workers synthesized a Pt/C catalyst with high-index facets such as (210), (310), and (510) exposed for Pt NCs [Zhou *et al,* 2010]. The synthetically scalable method for preparation of (111) dominated Pt-motif is nearly absent in these reports, with the exception of a few selective ones. Thus, this is an important requirement for the preparation of shaped Pt catalysts, which have higher active crystallographic planes.

3.1.3 Metal Loaded Polymer Supports

Heterogenization is usually obtained by binding of metal to the active part of the solid support under harsh conditions. The supporting materials should be thermally, chemically and mechanically stable during the reaction process. In these sequences, inorganic oxide [Vankelecom and Jacobs 2000, Lei *et al,* 2016], such as silica [Hong *et al,* 2015], zeolite, Al_2O_3 [Weng and Zaera 2014], ZrO_2, ZnO, clay and more recently carbon materials, are used as a support. These materials proved to be the best supporting materials, although with a few drawbacks such as, required high temperature for strong metal-oxide interaction [Tauster *et al,* 1978] and need for chemical activation before metal loading [Sharma and Sharma 2015]. To reduce the above extra efforts, it has been found that the organic and inorganic polymers are worthy supporting materials that require milder reaction conditions for metal-support

interaction [Bergbreiter 2000, Gruttadauria *et al,* 2008, Kristensen and Hansen 2010, Jumde and Mandoli 2016]. Thus, various metal supported polymer catalysts have been reported [Chauvin *et al,* 1977, Takeda *et al,* 2010] and have been used for asymmetric heterogeneous catalysis [Benaglia *et al,* 2003, Zhang and Riduan 2012]. Out of numerous heterogeneous polymer catalysts, impressive improvements have been made in a metal-polyamides system (Nylon 6, Nylon 66, Nomex and Nylon 610) due to their porous structure and geometry [Toy 1967, Yamaguchi *et al,* 1971]. Amide group of polymer helps to interact with the metal catalyst and the polymer skeleton influences product selectivity. Detailed studies on platinum, ruthenium, palladium and rhodium impregnated in polyamides have been studied in literatures [Teichner *et al,* 1982, Michalska and Ostaszewski 1986, Sermon and Azhari 1990].

3.1.4 Background of Selectfluor and F-CD-BF_4

Selectfluor has been used in many organic transformations like electrophilic fluorination, oxidative transformations of benzylic alcohols, allylation reaction of imine and functionalisation of aromatic systems [Burkart *et al,* 1997, Nyffeler *et al,* 2005]. The pH of the aqueous solution of Selectfluor (50 mg/ml) is around 3 [Liu and Wong 2002, Liu and Wong 2002]. It implicates the formation of N-H bond in water. These kinds of reactions are based on the fact that F-TEDA-BF_4 has considerable oxidative power, one of the strongest in the family of N–F reagents. Transfer of fluorine from Selectfluor to cinchonidine has been reported earlier [Shibata *et al,* 2000, Cahard *et al,* 2001]. The reason behind this is to develop a moiety that is capable of performing fluorination with selectivity. The fluorinated cinchonidine (F-CD-BF_4) proved to be a good selective fluorinating agent [Cahard and Audouard *et al,* 2001, Shibata *et al,* 2003]. Thus, it is an important task to prepare F-CD-BF_4 loaded carbon catalysts to use in organic transformations.

3.2 SYNTHESIS OF HETEROGENEOUS CATALYSTS

The heterogeneous catalysts were prepared using chiral polyamide and carbon materials like carbon nanotubes [Su 2011], graphene [Julkapli and Bagheri 2015], activated carbon [Jüntgen 1986, Addiego *et al,* 2016] and carbon fibers as supports [Fard and Mckay *et al,* 2016]. Information related to sample code, supplier and similar are displayed in table 3.1.

3.2.1 A Modified Impregnation Method for Preparing Metal Loaded Carbon Materials

A modified impregnation method was developed for the preparation of Pt loaded carbon materials (Figure 3.1). The activation process [Chen and Guan *et al,* 2011] consisting in refluxing the carbon materials (10 g) under constant stirring in HNO_3 (500 mL, 68 wt %) at 140 ˚C and are extracted by centrifugation at 3000 rpm. Carbon materials were washed several times with water followed by ethanol. The resultant materials were dried at 80 ˚C for 4 h under argon.

Table 3.1 Information related to sample code, supplier and similar

Samples	CAS / Product number	Specification	Supplier
Carbon nanotubes	308068-56-6	O.D.×L 6-9 nm× 5 µm	Sigma Aldrich
Graphene	799084	Black, Powder or Crystals or Flakes	Sigma Aldrich
Activated carbon	7440-44-0	Ash 4% max, Black powder	Alfa Aesar
Carbon fibers	NA	7 microns, Density = 1.81 ± 0.02 gm/cm^3	Auro carbon and chemicals
Chloroplatinic acid	18497-13-7	37 % assay Pt	Sigma Aldrich
Cinchonidine	485-71-2	White powder, Melting point 201-206°, Specific rotation = −109.2°(c = 1.5, Ethanol)	Alfa Aesar
Cinchonine	118-10-5	White powder, Mp = 253-258°, Optical Rotation: 260° ± 9° (c=2, 0.2M HCl)	Alfa Aesar
Camphoric acid	124-83-4	White crystals, Optical Rotation 44.0-48.0°(c = 1 % ,Ethanol)	Sigma Aldrich
Ethylene diamine	107-15-3	M.W. = 60.10, Colorless, Liquid	Sigma Aldrich
Tween 20	9005-64-5	Synonym = Polyethylene glycol sorbitanmonolaurate; Polyoxyethylenesorbitan monolaurate; Polysorbate 20	HIMEDIA

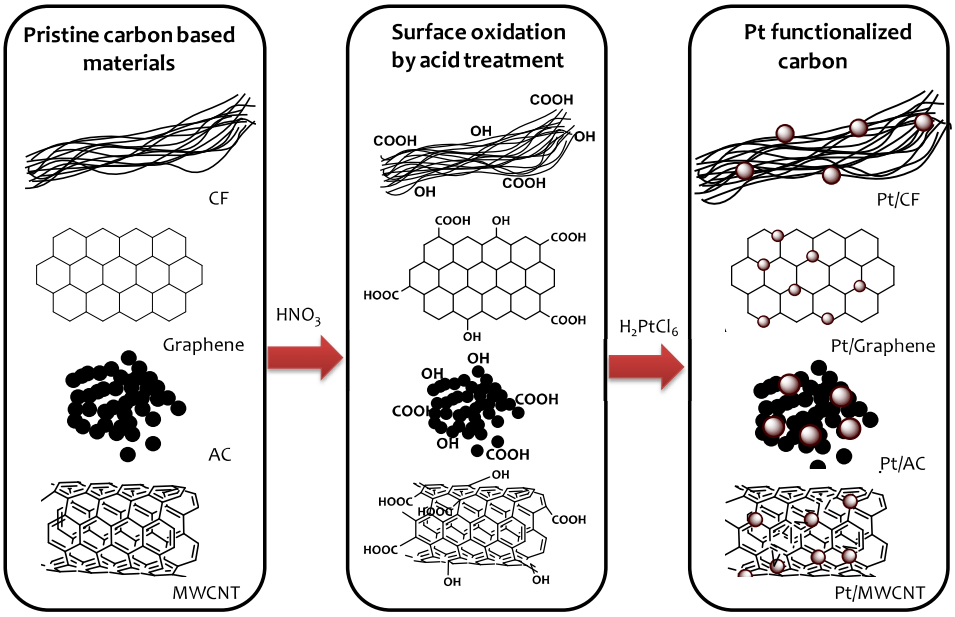

Figure 3.1 Graphical representations of activation process and Pt loading on carbon materials

A typical preparation experiment for Pt/MWCNTs was carried out (Figure 3.2) and a similar procedure was used for other metal loaded carbon materials (Table 3.2). The functionalized carbon materials were immersed in an ethanol solution under simultaneous stirring and sonication. Pt metal salt (H_2PtCl_6) was dissolved in degassed ethanol and added to carbon materials solution slowly via syringe pump under hydrogen bubbling for a period of 12 h. The solution is stirred for another 24 h, at room temperature, and finally heated at 100˚C, for 12 h. The platinum loaded carbon materials were isolated via centrifugation, followed by washing with deionised degassed water and dried at 80 ˚C, for 16 h, under argon.

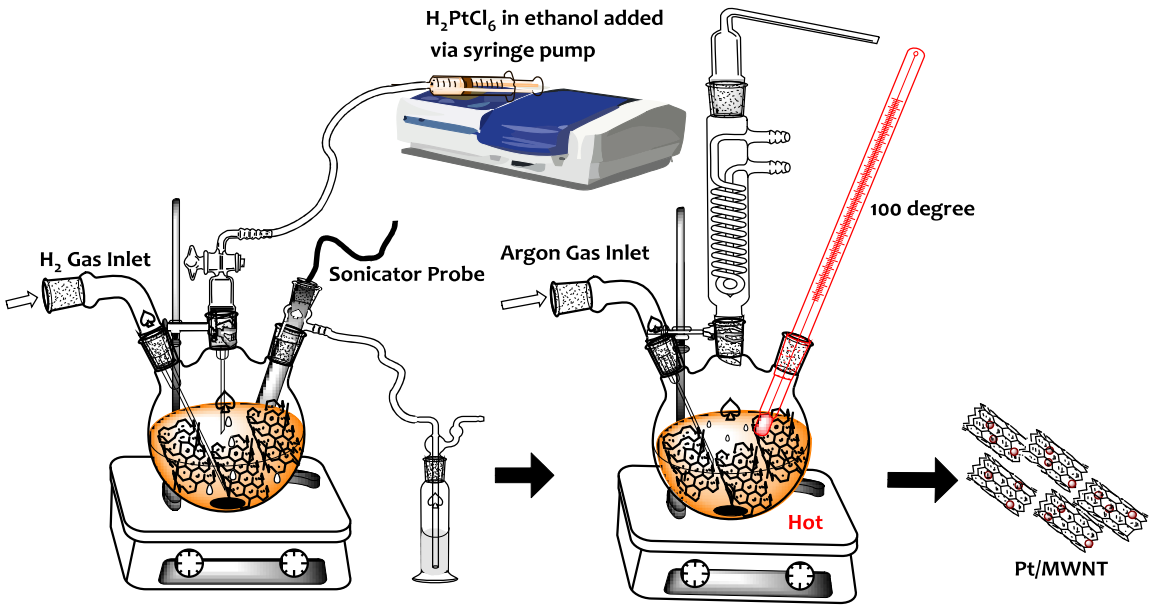

Figure 3.2 Graphical representation of the preparation of Pt loaded carbon nanotubes by a modified impregnation method

Table 3.2 List of catalysts prepared by the modified impregnation method

Entry	Catalysts codes
1	**(1a)** Co/MWCNT **(1b)** Co/Graphene **(1c)** Co/Carbon fiber **(1d)** Co/Activated carbon
2	**(2a)** Ni/MWCNT **(2b)** Ni/Graphene **(2c)** Ni/Carbon fiber **(2d)** Ni/Activated carbon
3	**(3a)** Pt/MWCNT **(3b)** Pt/Carbon fiber **(3c)** Pt/Graphene **(3d)** Pt/Activated carbon
4	**(4a)** Pt/TiO2/MWCNT **(4b)** Pt/TiO2/Graphene **(4c)** Pt/TiO2/Carbon fiber **(4d)** Pt/ZrO2/ MWCNT
5	**(5a)** Pd/ MWCNT **(5b)** Pd/Graphene **(5c)** Pd/Carbon Fiber
6	**(6a)** Cu/ MWCNT **(6b)** Cu/Graphene **(6c)** Cu/Carbon fiber
7	**(7a)** Tb/Graphene **(7b)** Tb/Carbon fiber **(7c)** Tb/MWCNT
8	**(8a)** Y/Graphene **(8b)** Y/Carbon fiber **(8c)** Y/MWCNT
9	**(9a)** Yb/Graphene **(9b)** Yb/Carbon fiber **(9c)** Yb/MWCNT
10	**(10a)** Gd/carbon Fiber **(10b)** Gd/Graphene **(10c)** Gd/MWCNT

3.2.2 Preparation of Pt HNC and Pt HNC Loaded Carbon Materials

A typical procedure of preparing Pt HNC/C is graphically presented in Figure 3.3. This process starts with the addition of H_2PtCl_6 (0.5 mmol; 0.210 g) in 5 mL water to make a clear yellowish solution which is added to 5 ml toluene in a 15 ml glass bottle (Figure 3.3a). The solution is thoroughly shaken for 5 min followed by adding of Tw20 (2 mL) to this solution. The mixture is further shaken until toluene layer turns to yellowish (Pt-organic precursor). The Pt-organic precursor layer is separated (Figure 3.3b) and added drop-wise to a suspended ethanol solution of functionalized carbon materials (2 g, 20 mL, Figure 3.3c) under sonication for around 1 h. The resultant Pt-Organic-Carbon solution is drop casted to a preheated glass disc at 130°C and maintained for 24 h under air (Figure 3.3d). The dried solid was washed with deionized water and ethanol to remove residual Tw20 (Figure 3.3e). The Pt loaded carbon catalyst was dried at 50°C and calcinated at 180 °C, for 24 h, to obtain Pt-HNC/C (1.9 g). List of prepared Pt HNC/C are tabulated in Table 3.3.

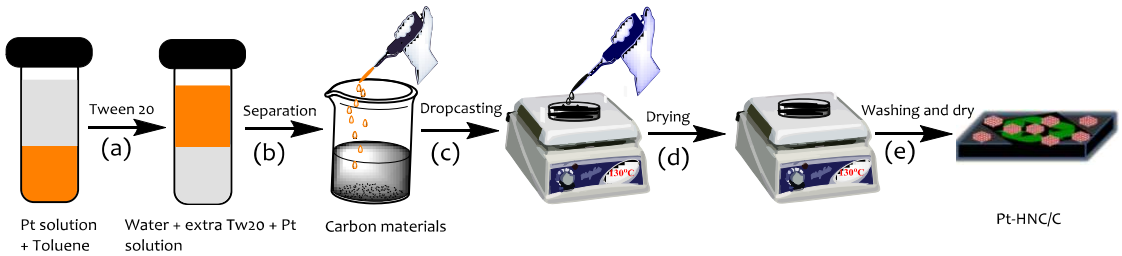

Figure 3.3 Graphical representation of the preparation of Pt HNC/MWCNT by using Tw20 phase transfer reagent

Table 3.3 List of catalysts prepared by the phase transfer process

Entry	Catalysts codes
1.	**(11)** Pt-HNC/ MWCNT
2.	**(12)** Pt-HNC/Carbon fiber
3.	**(13)** Pt-HNC/Graphene
4.	**(14)** Pt-HNC/Activated carbon

3.2.3 Preparation of Pt Loaded Chiral Polymer

Chiral polyamides were synthesized by interfacial condensation [Gonsalves *et al,* 1984] between chiral camphoric dichloride monomer, in an organic layer, and diamine monomer, in basic aqueous layer (Figure 3.4). Hexamethylenediamine (200 mg) was dissolved in water (5 mL) at 0˚C, adjusting the pH at 11 by adding aqueous NaOH. Chiral camphoric dichloride (200 mg) was dissolved in toluene (5 mL) and mixed with diamine solution at room temperature. The mixture was stirred at 80˚C for one hour. After the removal of solvent, a yellow gel (conversion > 99.9 %) was obtained, the gel was washed with toluene followed by n-hexane. Chiral polyamide (poly 5) was insoluble in most of the organic solvents but soluble in water and methanol (Table 3.4).

Table 3.4 Solubility tests of poly 5 carried out at room temperature

Solvents	Poly 5
Water	Soluble
Methanol	Soluble on Heating
Ethanol	Partially soluble
Toluene	Insoluble
n-Hexane	Insoluble
Cyclohexane	Insoluble
THF	Insoluble
Ethyl acetate	Insoluble
Acetonitrile	Insoluble
Chloroform	Insoluble

Chiral polyamide supported Pt was synthesized by a simple process (Figure 3.5) where chiral polyamide (10 mg) was dissolved in 1 mL of water. The homogeneous solution was poured into a Teflon stencil (20 ×20 ×1 mm^3 dimension) and placed in a vacuum oven overnight at 120˚C, to evaporate the water, on a yellowish colored film (Figure 3.5b). Platinum solution (5 wt%, H_2PtCl_6) was dispersed on the chiral polyamide film and placed in a high pressure reactor for 2 h in H_2 pressure, at 50 ˚C, to reduce the Pt metal (Figure 3.5c). The Pt loaded chiral polyamide film was washed with n-butanol and used for catalytic reactions. Other chiral polyamides (poly 1-4) and catalysts (I-IV) were prepared by varying diamine monomers like ethylenediamine, 1, 3 diaminopropane, 1, 4 diaminobutane and 1, 5 diaminopetane which are tabulated in Table 3.5.

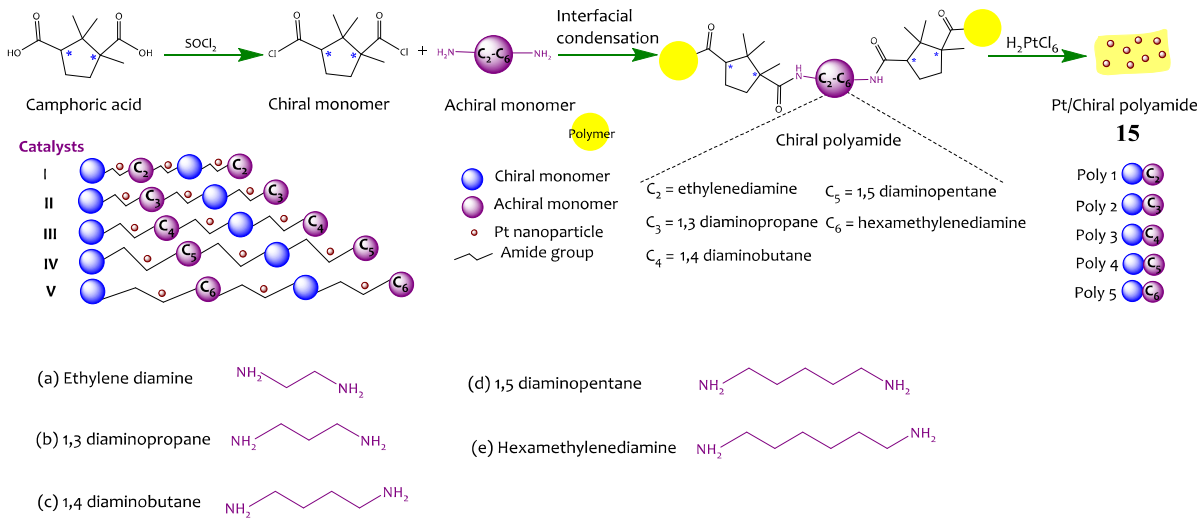

Figure 3.4 Typical preparations of various chiral polyamide and Pt/Chiral polyamide compounds

Table 3.5 List of polyamides and catalysts prepared by interfacial condensation reaction

S. No.	Chiral monomer	Achiral monomer	Polyamide	Catalysts
1	D-camphoric acid	Ethylenediamine	Poly 1	Catalyst 1 **(15a)**
2	D-camphoric acid	1,3 diaminopropane	Poly 2	Catalyst II **(15b)**
3	D-camphoric acid	1, 4 diaminobutane	Poly 3	Catalyst III **(15c)**
4	D-camphoric acid	1, 5 diaminopetane	Poly 4	Catalyst IV **(15d)**
5	D-camphoric acid	Hexamethylenediamine	Poly 5	Catalyst V **(15e)**

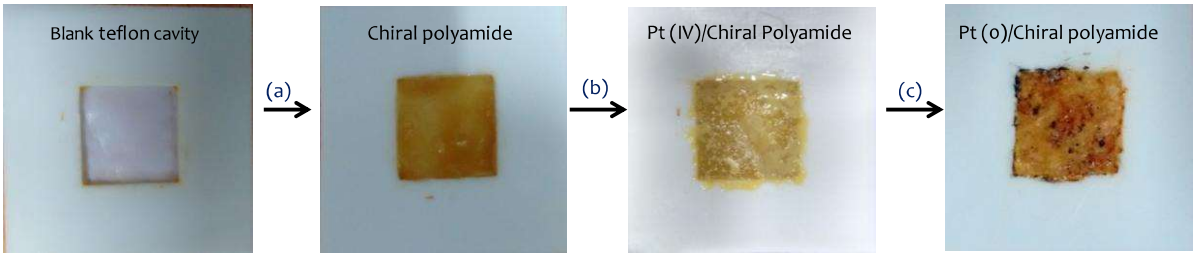

Figure 3.5 Images of catalyst preparation (a) Aqueous solution of chiral polyamide added to Teflon stencil, (b) Aqueous H_2PtCl_6 solution added to chiral polyamide, and (c) Reduction of Pt (IV) to Pt (o) using high pressure hydrogen

3.2.4 Preparation of F-CD-BF_4 and F-CD-BF_4 /Pt/MWCNT

(a) Preparation of F-CD-BF_4

F-CD-BF_4 was prepared by a previously reported method [Shibata and Suzuki *et al,* 2000, Cahard and Audouard *et al,* 2001], in which mixing an equimolar amount of cinchonidine and Selectfluor in acetonitrile was carried out at room temperature (Figure 3.6). The mixture is stirred for 15-20 min. The reaction was completed after 20 minutes and the product was analyzed by ^{19}F NMR. F-CD-BF_4 was purified by a $C_2H_6CO + H_2SO_4$ mixture.

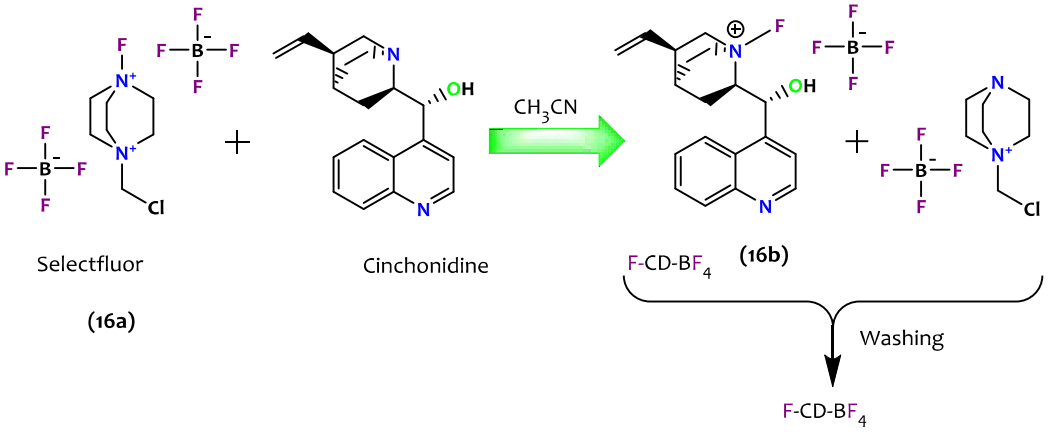

Figure 3.6 Preparation of F-CD-BF_4

(b) Preparation of F-CD-BF_4 /Pt/MWCNT

The synthesis of F-CD-BF_4/Pt/MWCNT and F-CD-BF_4/MWCNT was carried out. Pt loaded MWCNT (3a) solution (prepared in Figure 3.2) was mixed with F-CD-BF_4 in acetonitrile, and stirred for 1 h, at 80°C. The resulting mixture was washed with ethanol, followed by calcinations at 120°C. F-CD-BF_4 was loaded (10% wt) on MWCNT and Pt/MWCNT.

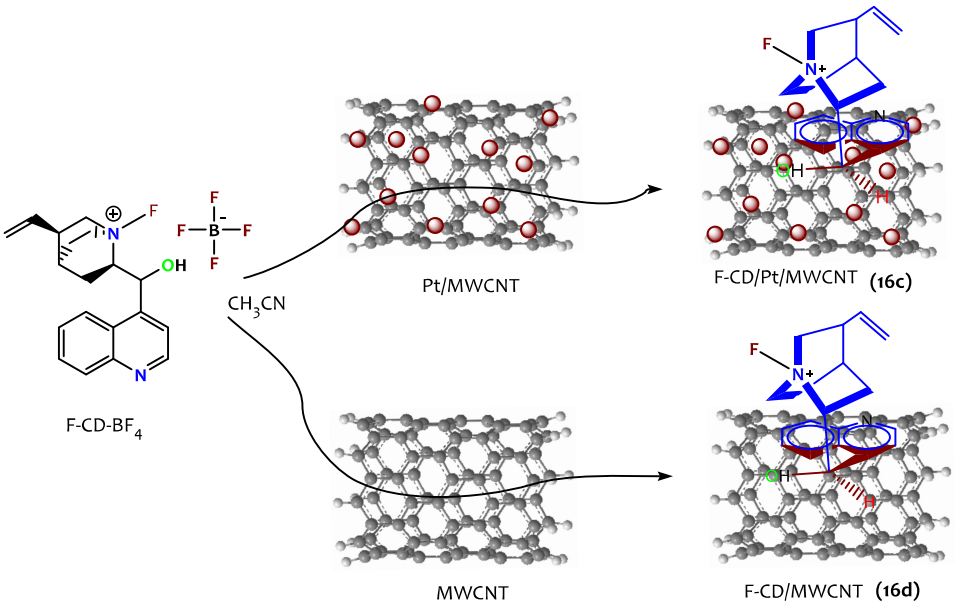

Figure 3.7 Preparation methods of F-CD-BF_4/Pt/MWCNT and F-CD-BF_4/MWCNT

3.3 CHARACTERIZATION

3.3.1 SEM Analysis

Scanning electron microscopy (SEM) is a useful technique to investigate the topography and morphology of micro and nano-structured materials. This instrument uses a powerful beam of electrons (produced by a thermionic or field emission technique) to illuminate the sample and then project images based on the secondary or back-scattered electrons collected by the detector after scanning. The morphology of different samples was analyzed using scanning electron microscopy (SEM, EVO18 Ziess) after spreading the catalyst powder onto a conductive silver tape and then put in the vacuum chamber with an accelerating voltage of 20 KeV.

3.3.2 TEM Analysis

Transmission electron microscopy (TEM) is a high resolution technique for producing high resolution images, crystal structure, atomic arrangements, exposed crystal facets and chemical compositions. Samples are illuminated by a high energy electron beam which passes through several condensers and then is transmitted to the sample. Electrons can be scattered elastically or inelastically based on diffraction theory and then collected, electrons are processed to produce images. Transmission electron microscopy (TEM) was carried out in a FEI Tecnai-G^2 T20. For TEM study, the catalysts were dispersed in a solvent (ethanol) using tip ultrasonication and a droplet of suspension was placed on to a copper grid and dried in air.

3.3.3 EDX Analysis

Energy dispersive x-ray spectroscopy (EDX) can be carried out simultaneously with a common imaging technique by adding an EDX detector to a SEM or TEM unit. When electrons bombard a material surface of interest, X-rays are also emitted and can be collected by the EDX detector. The energy of the X-rays and their corresponding intensities are related to the appropriate elemental identity and quantity in a specific material. Moreover, elemental mapping can also be done by analyzing the X-rays emitted from localized positions on the sample. Atomic contents depend on the emitted X-ray intensities at various locations and can be used to map the concentration of different elements over the entirety of the sample being investigated.

3.3.4 X-ray Diffraction

X-ray diffraction (XRD) is a characterization technique used to determine crystal structures, average nanoparticles size and lattice parameter along with the crystal phases. Generally, X-ray beams are emitted from a source (Cu, K, Mo, etc.) and directed to the sample of interest. Once these beams interact with the atoms of the materials, a diffraction pattern of a specific crystal structure can be obtained, depending on the incident X-ray wavelength and the spacing between the atomic planes in crystalline and polycrystalline materials. An X-ray diffractometer, D8 advance (Bruker, U.S.A.) using Cu Kα1 (λ = 1.54056 Å) as a radiation source was used to ascertain the quality and crystalline nature of samples with tube current and voltage of 40 mA and 40 kV, respectively.

3.3.5 Raman Spectroscopy

Raman spectroscopy is a useful technique to obtain the information of rotational and vibration modes in a system. The Raman Effect which is small, but accessible by the use of lasers, involves the interaction of the monochromatic laser light with the molecular vibrations, photons or other excitations in the sample and the resulting shift in the energy of the laser photons. This shift in energy provides information about the vibration modes in a sample. In this study, Raman spectroscopy is used as an important characterization tool for the investigation of defected sites in carbon materials. Raman spectra of samples were performed at room temperature using Renishaw instruments with an emission wavelength of 532 nm.

3.3.6 UV-Vis Spectroscopy

UV-Vis spectroscopy is used to determine the organic compounds, transition metal ion and biological molecules. UV-Vis spectroscopy measurement was carried on Varian Cary 4000 in the range of 200-800 nm.

3.3.7 CV Analysis

Cyclic voltammetry (CV) is a potentiostatic electrochemical technique used to examine the electrochemical properties of electrodes. In a cyclic voltammetry test, the potential of the working electrode is varied linearly between two potential limits with respect to time and the corresponding current is measured. The electrochemical activity of Pt/C catalysts was analyzed in oxygen reduction reaction by cyclic voltammetry (CH Instruments, electrochemical workstation).

3.3.8 FTIR Spectroscopy

Fourier transform infrared spectroscopy (FTIR) is a technique which is used to obtain an infrared spectrum of absorption or emission of a solid, liquid or gas. Fourier-transform infrared spectra (FTIR) were recorded on a Vertex 70v spectrometer (Bruker) in the range of 400-4000 cm^{-1}.

3.3.9 AFM Analysis

Atomic force microscope (AFM) is used to determine some properties of sample like morphology, friction, magnetism and height. It is a kind of scanning probe microscope (SPM) and to acquire an image, the probe scans over a small area of the sample. Atomic force microscopy (AFM) was recorded from park XE-70.

3.3.10 NMR Spectroscopy

NMR spectroscopy is technique that allows the sequential analysis of a large number of different atoms like ^{31}P, ^{29}Si, ^{11}B, ^{19}F, ^{7}Li and ^{195}Pt. Nuclear magnetic resonance spectra (1H NMR) were recorded on a Bruker 500 spectrometer operating at 500 MHz in a deuterated solvent.

3.3.11 HPLC Analysis

High performance liquid chromatography (HPLC) technology is used for the separation of product and chiral compound. The principal of this technique is to separate the product mixed in mobile phase on the surface of the stationary phase on the basis of retention time [Pirkle and House 1979]. HPLC chromatograms were recorded on WATERS system, Ireland.

3.3.12 TGA Analysis

TGA is a method of thermal analysis in which changes in physical and chemical properties of materials are measured as a function of increasing temperature (with constant heating rate), or as a function of time [Coats and Redfern 1963]. Thermogravimetric analyses were performed on a TGA-6000 thermal analyzer (Perkin Elmer), under a nitrogen atmosphere (19.8 mL/min flowing nitrogen, a temperature range of 30-900˚C and pressure 3 bars) and a heating rate of 10 ˚C min^{-1}.

3.3.13 BET Analysis

BET equation is used to determine the surface area, pore volume and pore size distribution of materials. Surface area and pore size measurements of Pt loaded support materials were carried out on standard nitrogen adsorption equipment (Quantachrome autosorb iQ3), at 196˚C, using N_2 gas with 99.99% purity.

3.3.14 CD Analysis

In order to evaluate the optical activity and architecture of chiral polyamide, UV and CD spectroscopic analyses were carried out. The CD spectra were obtained from a circular dichroism (JASCO, J-815 CD-Spectrometer), in N_2 atmosphere, in the wavelength range of 200-800 nm, using a quartz cuvette cell.

3.3.15 GPC Analysis

Polyamide molecular weight and weight distributions (Dispersity, M_w/M_n) were determined by gel permeation chromatography (GPC, Water alliance 2690 and detector RI 2140), using polyethylene glycol standard, at 30 °C, with a flow rate of 1.0 mL/min.

3.4 RESULTS AND DISCUSSION

3.4.1 SEM and EDX Analyses of Catalysts

(a) Pt Loaded Carbon Support

Figure 3.8 shows the SEM images recorded for carbon materials and Pt loaded carbon materials. In the case of activated carbon, shows heterogeneous pores in a honeycomb shape (Figure 3.8a). After Pt loading on activated carbon, the Pt nanoparticles are seen as well distributed in the pores of activated carbon (Figures 3.8b and c). Figure 3.8d shows the smooth morphology of carbon fibers, while after loading of Pt, Figures 3.8e and f show that Pt nanoparticles are uniformly distributed on the fibers surface. In Figure 3.8g, the morphology of graphene is found to be like the petals of a flower. Further, Pt loaded graphene is shown in Figures 3.8h and I, in which Pt nanoparticles are well disseminated on the petals of graphene. Further, Figures 3.8j and k show bundles of carbon nanotubes, where individual nanotubes are well distinguished from each other. After loading of Pt, nanoparticles are found on the surface of carbon nanotubes. The particles are not aggregated, which might be a good indication for asymmetric catalysis. All SEM images were obtained in the range of 3 µm to 500 nm. Pt nanoparticles in nanocomposites are recognized as white bright dots, which confirm that the Pt incorporation process was successful. The EDX analysis confirmed the Pt loading. The element mapping is shown in Figure 3.9.

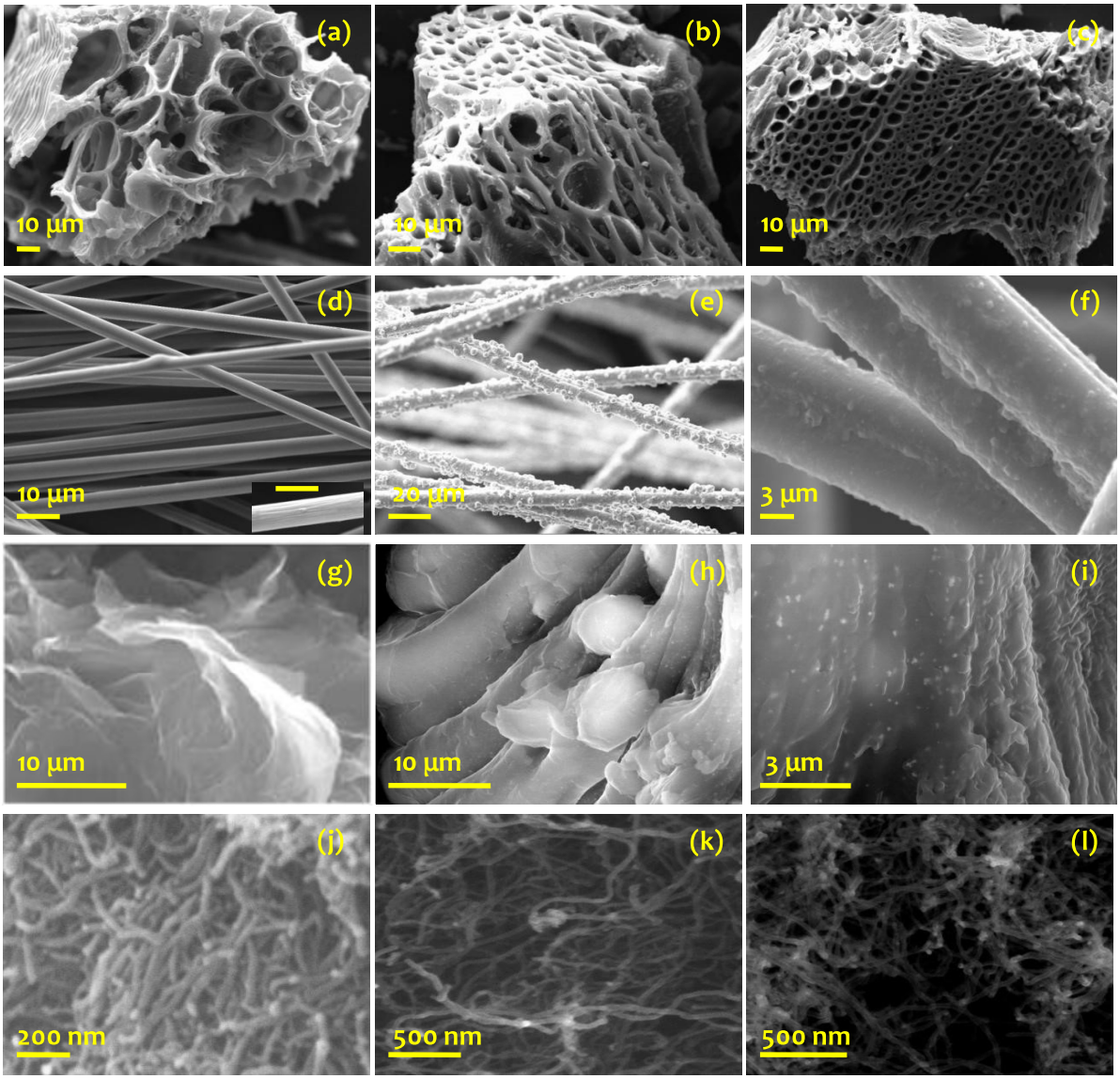

Figure 3.8 SEM images of (a) activated carbon, (b, c) Pt/AC, (d) CF, (e, f) Pt/CF, (g) graphene, (h, i) Pt/graphene, (j, k) MWCNT, and (l) Pt/MWCNT

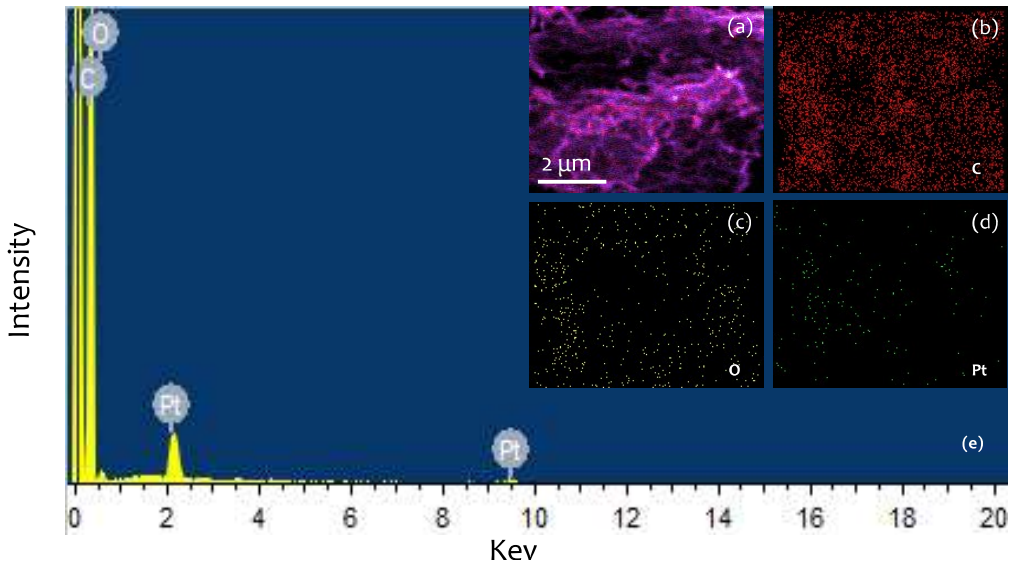

Figure 3.9 EDX mapping of (a) Carbon nanotube, (b) Carbon, (c) Oxygen, (d) Pt, and (e) Spectrum of carbon nanotube

(b) Pt Loaded Chiral Polyamide

The morphology of chiral polyamide and distribution of Pt nanoparticles on polyamide were characterized by field emission scanning electron microscopy (FESEM, Figure 3.10). Chiral polyamide displays a nanofibrous network layer morphology, as shown in Figures 3.10a and b. In Pt loaded chiral polyamide; the Pt nanoparticles are uniformly dispersed on a layer of chiral polyamide and have similar nanoparticles sizes (Figures 3.10c, d, e and f). The EDX mapping and spectrum of Pt/Chiral polyamide is confirmed well distribution, and presence of atomic platinum on the polyamide surface (Figure 3.11).

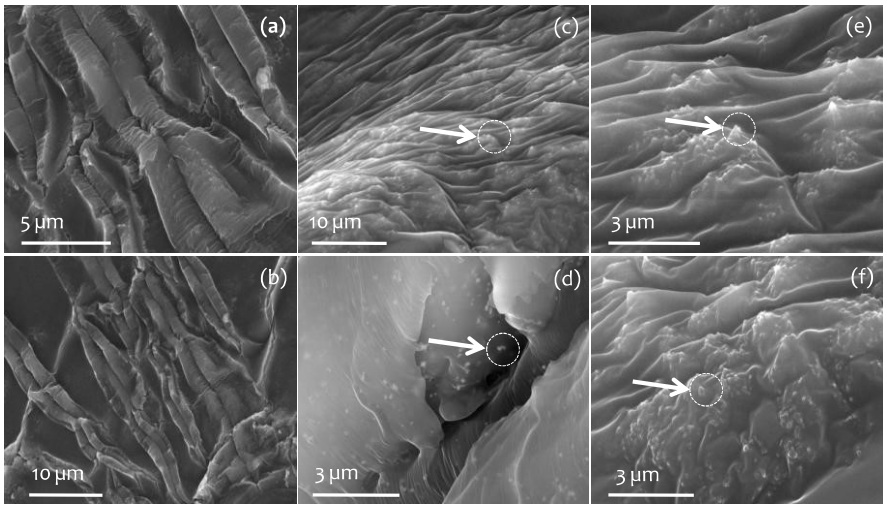

Figure 3.10 SEM images of (a, b) Chiral polyamide and (c, d, e and f) Pt/Chiral polyamide

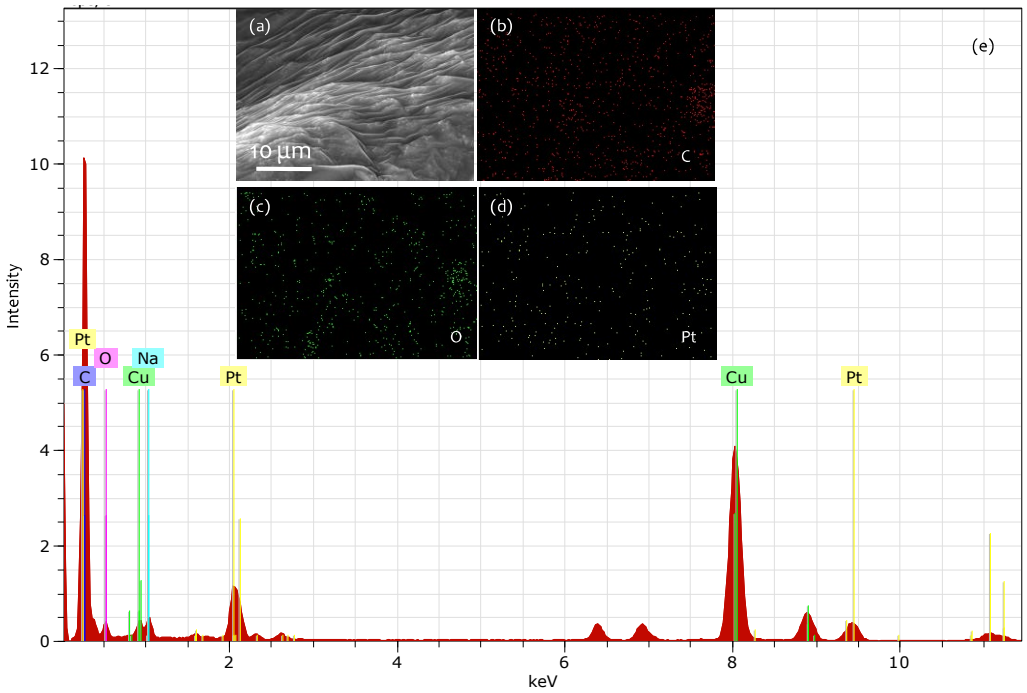

Figure 3.11 EDX mapping of (a) Pt/Chiral polyamide, (b) Carbon, (c) Oxygen, (d) Pt, and (e) Spectrum of Pt/Chiral polyamide

(c) Selectfluor, F-CD-BF_4 and F-CD-BF_4/Pt/MWCNT

The morphology of Selectfluor, F-CD-BF_4, F-CD-BF_4/MWCNT and F-CD-BF_4/Pt/MWCNT was characterized using SEM. Selectfluor and fluorinated cinchonidine shows heterogeneity in morphology as depicted in Figures 3.12a and b. F-CD-BF_4 loaded carbon nanotubes shows heterogeneity at 10 µm, but at higher magnification carbon nanotubes can be easily identified along with fluorinated cinchonidine (Figures 3.12c and d). Morphology of F-CD-BF_4/Pt/MWCNT is similar to F-CD-BF_4 loaded carbon nanotubes (Figures 3.12e and f). The good distribution of F-CD-BF_4 on MWCNT is represented in Figure 3.13. The presence of fluorine was confirmed by EDX spectrum (Figure 3.13e).

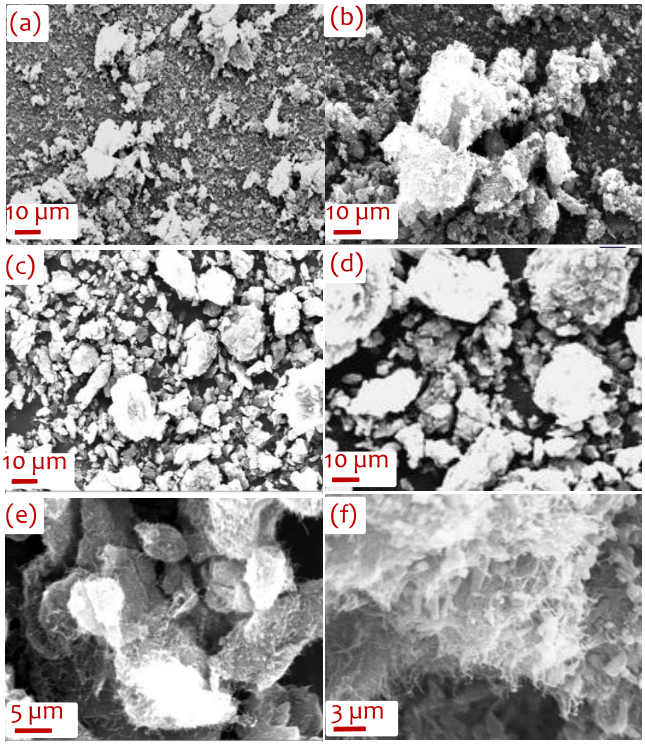

Figure 3.12 SEM images of (a) Selectfluor, (b) F-CD-BF_4, (c, d) F-CD-BF_4/MWCNT, and (e, f) F-CD-BF_4/Pt/MWCNT

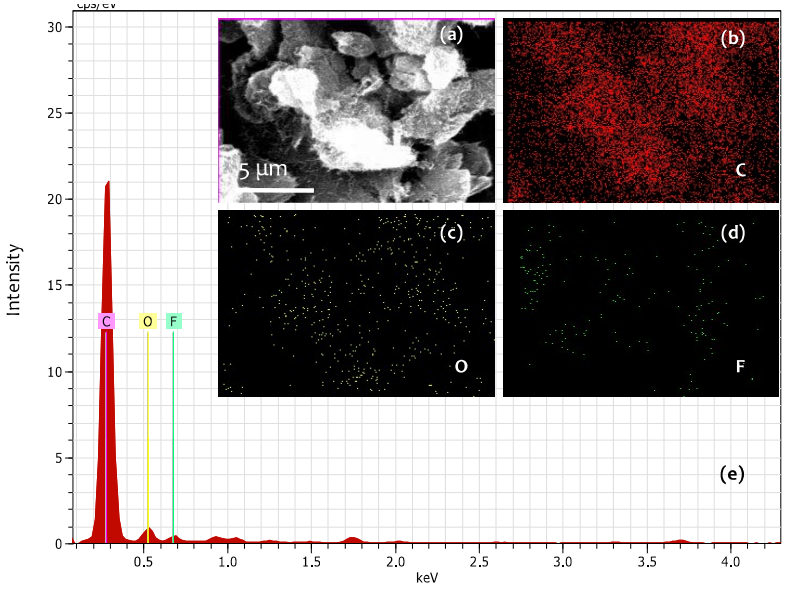

Figure 3.13 EDX mapping of (a) F-CD-BF_4/MWCNT, (b) Carbon, (c) Oxygen, (d) Fluorine, and (e) Spectrum of F-CD-BF_4/MWCNT

3.4.2 HRTEM Analysis of Catalysts

(a) Pt Loaded Carbon Support

The HRTEM images show that the Pt nanoparticles are extremely small in size (2-20 nm) and highly dispersed, given the high surface area of carbon materials (Figure 3.14). The nanoparticles are homogeneously dispersed in case of activated carbon, which leads to interactions between the carbon surface and the Pt nanoparticles. Figure 3.14b shows the Pt loaded carbon fibers, and indicates that Pt nanoparticles are well attached on the surface of carbon fiber. In Pt/Graphene, Pt nanoparticles are well distributed on graphene sheet and have heterogeneity in size (Figure 3.14c). Figure 3.14d shows Pt nanoparticles loaded carbon nanotubes indicating that the Pt nanoparticles are found on the inside and outside surface of a carbon nanotube. MWCNTs provide more reduction sites due to the higher surface area as CNTs have a cylindrical structure and the pores result from the free space in the bundles [Carabineiro *et al,* 2013].

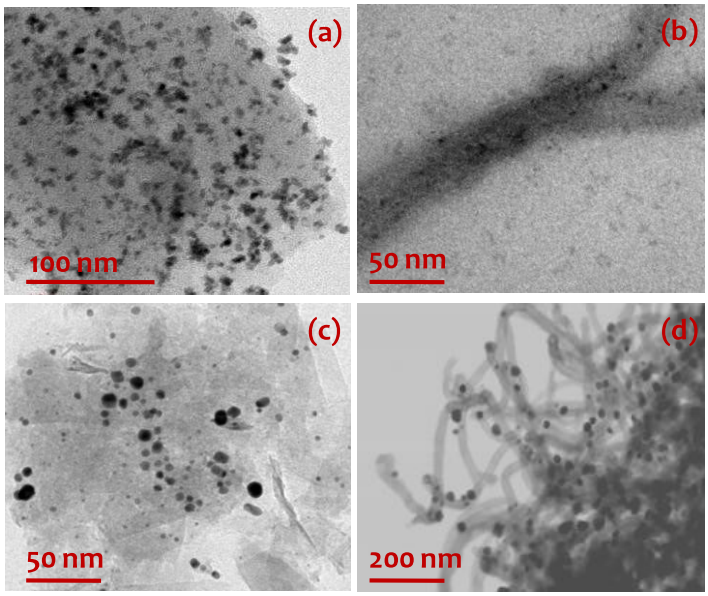

Figure 3.14 TEM images of (a) Pt/AC, (b) Pt/CF, (c) Pt/Graphene, and (d) Pt/MWCNT

(b) Pt HNC Loaded Carbon Materials

The HRTEM images, shown in figure 3.15, show the shape and distribution of Pt nanocrystals on carbon materials. There are differences in the outer and inner surface of the tubes as shown in Figure 3.15a. Pt NCs are disseminated on the carbon materials, being hexagonal in shape, with a high degree of (111) facets. As shown in Figure 3.15a, Pt nanocrystals are found on outer and inner surface of carbon nanotubes. The Pt nanocrystals deposited on graphene also have a hexagonal shape, as shown in Figure 3.15b. An isolated Pt HNC could behave like a single atom catalytic site. The higher magnification TEM images of Figure 3.15d and e provides further information about the shape and allocation of hexagonal nanocrystals on the surface of carbon materials. The HRTEM also shows Pt (111) lattice fringes with spacing of 0.23 nm parallel to the outer surface of the nanocrystals (Figure 3.15d).

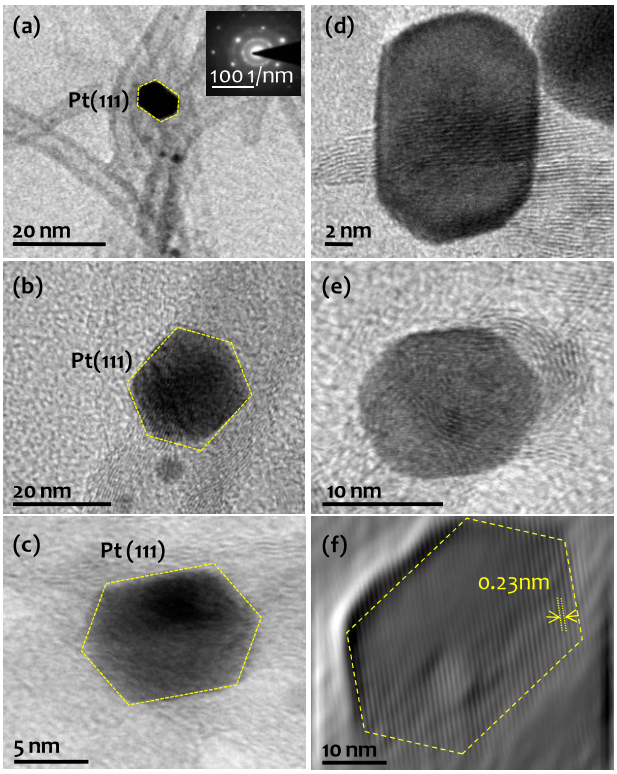

Figure 3.15 HRTEM images of (a and d) Pt HNC/ MWCNT, (b and e) Pt HNC/Graphene, (c) Pt HNC/ CF, and (f) A FFT high resolution lattice fringes of Pt(111)

(c) Pt Loaded Chiral Polyamide

HRTEM images present the morphology of chiral polyamide and dispersion of Pt in catalysts l-IV (Figure 3.16). The chiral polyamide has a helical shape, as observed in CD spectra. Pt nanoparticles are well dispersed at a particular distance in a helical polyamide (Figures 3.16a-e). The uniform dispersion of Pt nanoparticles is observed at higher magnification (Figures 3.16f-i) and it is observed that the distance between nanoparticles increases with the number of carbon atoms between the two amino groups of diamine (Figure 3.16), with a comparable particle size of Pt (2-6 nm) (Figures 3.16a, c and e). These isolated particles may behave like single atoms with 0.23 nm interplaner distance (Figures 3.16b, d and f). Lattice fringes with a spacing of 0.23 nm, parallel to the outer surface, indicate a FCC crystal structure of Pt metal, in which the (111) facet is predominant.

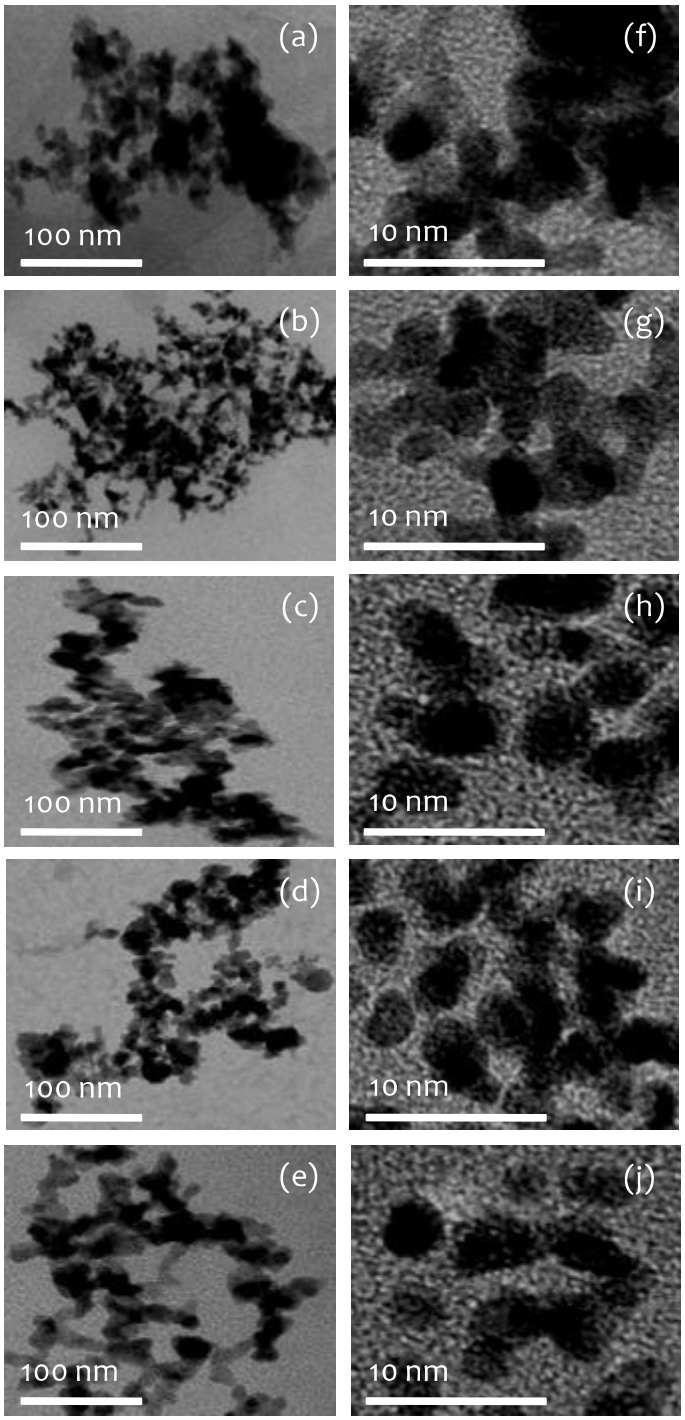

Figure 3.16 HRTEM images of (a-e) catalysts I-IV, (15 a-e) 100 nm, and (f-j) 10 nm

(d) Selectfluor, F-CD-BF_4 and F-CD-BF_4/Pt/MWCNT

The HRTEM demonstrates the morphology and loading status of F-CD-BF_4 on carbon nanotubes. Figure 3.17a shows the images of Selectfluor loaded carbon nanotubes in which they make spider net composites with Selectfluor. Figure 3.17d shows that the F-CD-BF_4 is fixed on carbon nanotubes and forms a similar composition. The HRTEM images of F-CD-BF4/Pt/MWCNT are presented in Figure 3.17e. The distribution of metal on carbon nanotubes is shown in Figure 3.17f and it can be observed that metal nanoparticles are located outside and inside the surface of carbon nanotubes. The shape of nanoparticles is observed at higher magnification (Figures 3.17f, g and i).

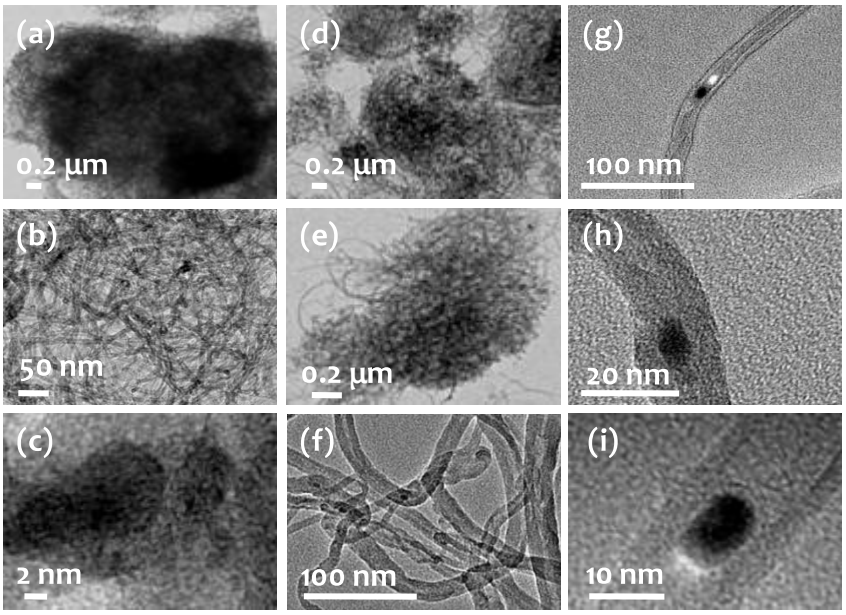

Figure 3.17 HRTEM images of (a, b, and c) Selectfluor/MWCNT, (d, e) F-CD-BF_4/MWCNT, and (f, g, h and i) F-CD-BF_4/Pt/MWCNT

3.4.3 XRD Analysis of Catalysts

(a) Pt Loaded Carbon Materials

Functionalized carbon supports and Pt loaded carbon materials are characterized using XRD as shown in Figure 3.18. The XRD results are similar to previous studies dealing with Pt loaded carbon materials [Li *et al,* 2003, Xing 2004]. The XRD pattern for functionalized carbon shows an intense peak at 25.90˚ along with other peaks at 42.70˚ and 53.50˚ corresponding to the (002), (100), (004) reflections from graphitic carbon, respectively. Carbon materials with more graphitic character show more intense reflection from (002) plane. The Pt loading results in three major peaks at 39.68˚, 46.4˚ and 67.7˚ corresponding to the diffractions of from the (111), (200) and (220) planes of the face-centered cubic (FCC) lattice of Pt nanoparticles. The typical form of the FCC Pt structure indicates effective reduction of the metal precursor. Nevertheless, the (100) related to carbon disappears after the loading of Pt nanoparticles. The XRD analysis confirms that the carbon material retains its structural planes even after functionalisation.

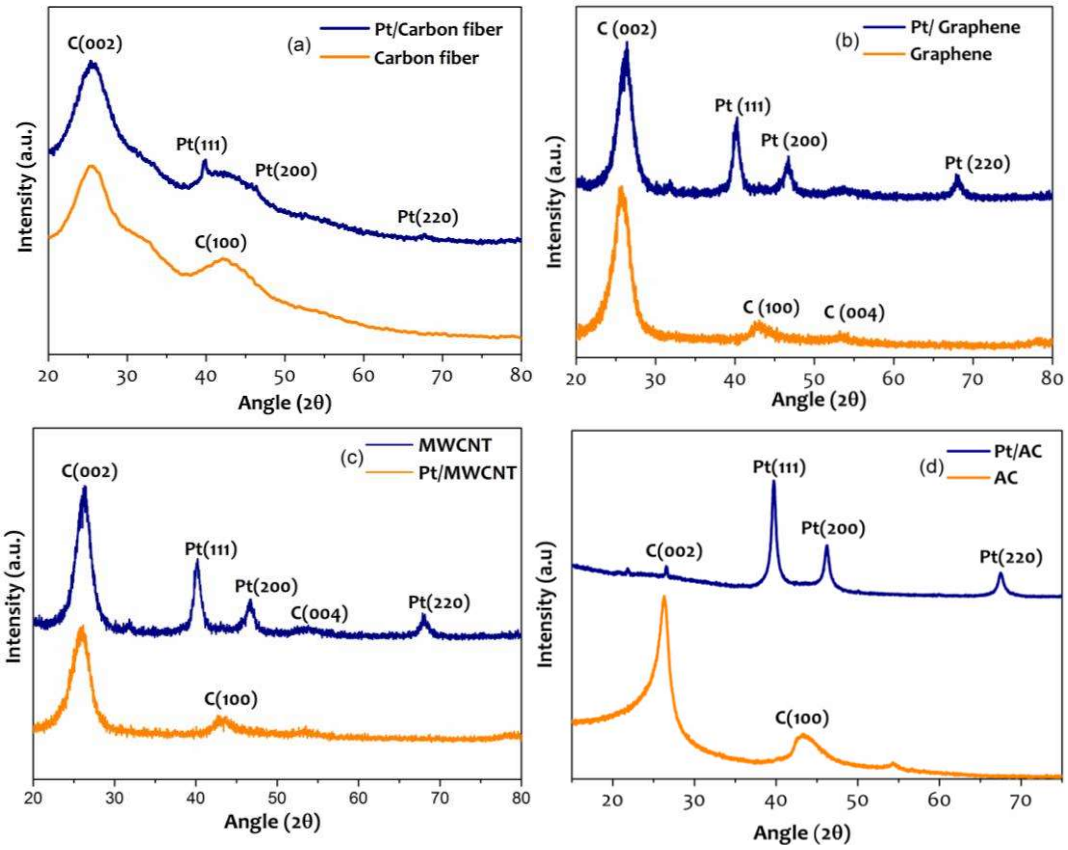

Figure 3.18 XRD patterns of (a) Carbon fiber and Pt/CF, (b) Graphene and Pt/Graphene, (c) MWCNT and Pt/MWCNT, and (d) Activated carbon and Pt/Activated carbon

(b) *Pt HNC Loaded Carbon Materials*

The Pt hexagonal nanocrystals show three major peaks at 39.68˚, 46.4˚ and 67.7˚, corresponding to the diffractions from the (111), (200), and (220) planes of Pt nanoparticles indicating FCC crystal structure of Pt metal with predominance of (111) facets (Figure 3.19a). Graphitized carbon peaks also appear in XRD patterns after loading of Pt HNC on carbon materials (Figure 3.19b).

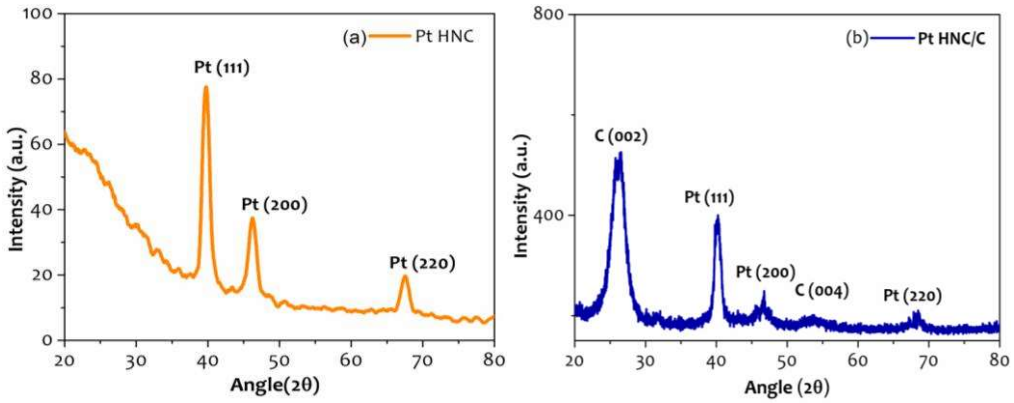

Figure 3.19 XRD patterns of (a) Pt HNC, and (b) Pt HNC/C

(c) Pt Loaded Polyamide

Chiral polyamide film and catalysts are characterized using XRD as shown in Figure 3.20. The XRD pattern of the pristine polyamide nanofibers exhibited at 30.2˚, tells the presence of different phases of polymer (Figure 3.20a). The catalyst V shows peaks at 39.6˚, 46.4˚, 67.7˚ and 81.2˚ corresponding to the diffractions from the (111), (200) and (220) planes of a crystalline face-centered cubic (FCC) lattice of Pt, with a dominating intense peak of Pt (111) (Figure 3.20b). Other catalysts showed similar XRD patterns in XRD analysis.

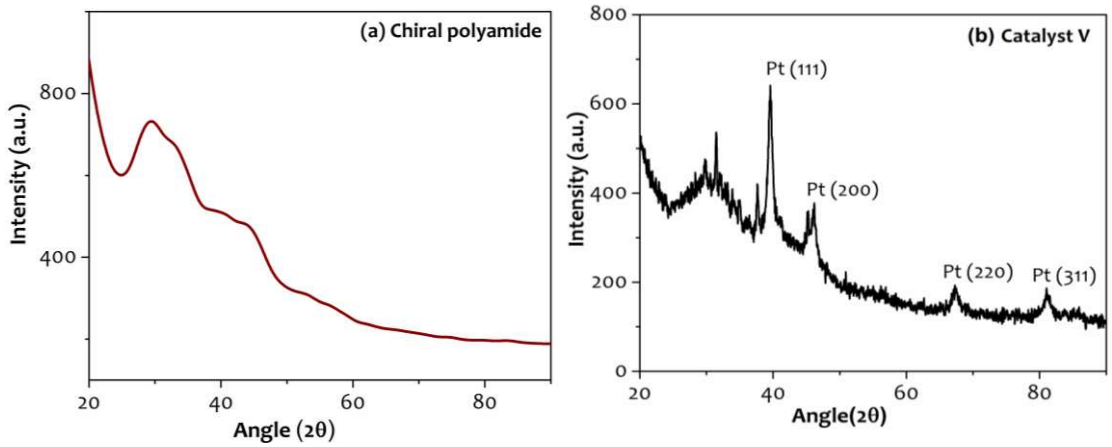

Figure 3.20 XRD patterns of (a) Chiral polyamide, and (b) Catalyst V

3.4.4 AFM analysis of Catalysts

Pt Loaded Carbon Materials

AFM is used to determine 1D and 3D morphology of the samples (Figure 3.21). The samples were prepared via drop casting, in which a well sonicated homogeneous solution was dropped on mica, followed by dehydration at 60˚C. Samples were scanned at various scan size in non-contact mode. The Figure 3.21a, Pt loaded MWCNTs bundles are observed. Figure 3.21d gives information about the length and approximate valuation of the diameter of nanotube, and attachment of metal particles. It is impossible to determine the accurate value of the diameter of a nanotube because only a few nanotubes were directly attached to mica. Graphene layered structure is seen in Figures 3.21b and c. The 3D image of graphene confirmed the layered structure. In case of Pt loaded CF, Pt particles is stacked on a fiber surface. Metal particle size is measured from Figure 3.21c & f. Carbon fibers have greater roughness among the three carbon materials. Thus, Pt loading is higher with low dispersion on carbon fibers.

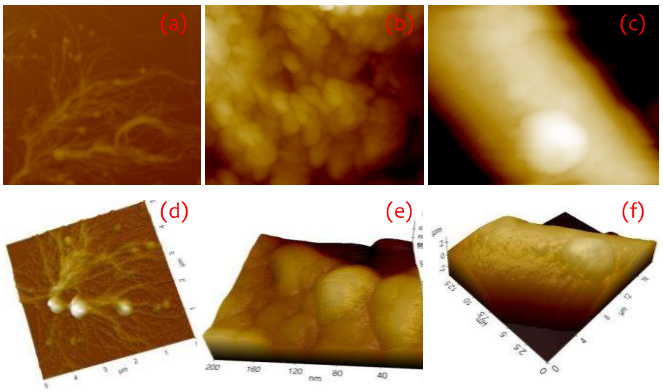

Figure 3.21 1D and 3D AFM images of (a and d) Pt/MWCNT, (b and e) Pt/graphene, and (c and f) Pt/CF

3.4.5 CV Analysis of Catalysts

Pt Loaded Carbon Materials

Electrochemical activities are compared between blank glass electrodes, functionalized carbon materials and Pt loaded carbon catalysts in Figure 3.22. Background of cyclic voltammetry was collected in 0.5 M H_2SO_4 (saturated with oxygen) for blank glass electrode. Functionalized carbon materials and Pt/C with nafion solution were made and pasted on a glass electrode. The activities were scanned between - 0.21 and 1.2 V potential for functionalized carbon materials and Pt/C at 50 mV/s, where Pt/C showed maximum electrochemical activity, with oxygen reduction due to the presence of Pt metal. No oxygen reduction was observed in the absence of Pt metal. Functionalized carbon materials showed higher activity than glassy carbon electrode due to their higher surface area. The glassy carbon electrode does not show electro chemical activity.

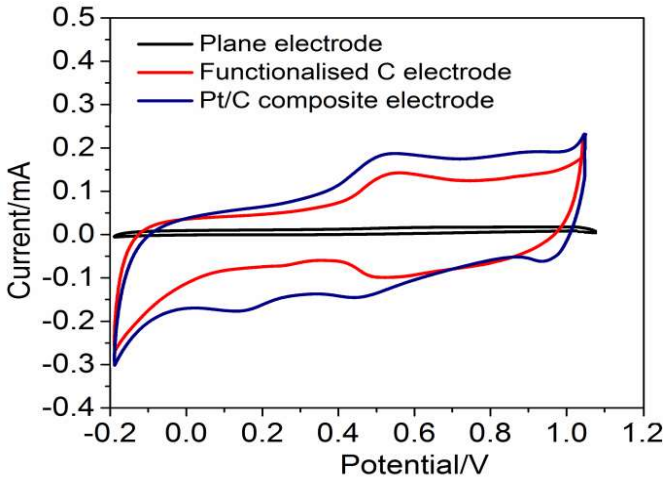

Figure 3.22 CV response of plane electrode, functionalised carbon materials and Pt loaded carbon materials

3.4.6 FTIR Analysis of Catalysts

(a) Functionalised Carbon Materials and Pt Loaded Carbon Materials

IR spectra were taken for all metal loaded carbon materials. Measurements were performed under transmission mode. The IR spectra of functionalized carbon materials and Pt loaded carbon materials are shown in Figure 3.23. In case of functionalized carbon materials, Figure 3.23a shows some characteristics peaks around 400 and 700 cm^{-1} of aromatic C-H bending (699.23 cm^{-1}). Other peaks like 1547.07, 1696.21, 2356 and 3600-3700 cm^{-1} come due to C-C stretching, six member C=O stretching, C=C stretching and O-H functional group, respectively. The IR spectrum of Pt loaded carbon materials nanocomposites depicted in Figure 3.23b show some new peaks which are assigned to the carboxylic ion binding between nanoparticles and the carbon materials. Other new peaks, like 1727.52 cm^{-1} and 3331.11 cm^{-1}, are attributed to aromatic C=C stretching and O-H stretching, respectively. The peak appearing at 839.86 cm^{-1} (Pt-O covalent bond Pt (111)) could be attributed to a strong bond between the Pt and the carbon materials through an oxygen containing group.

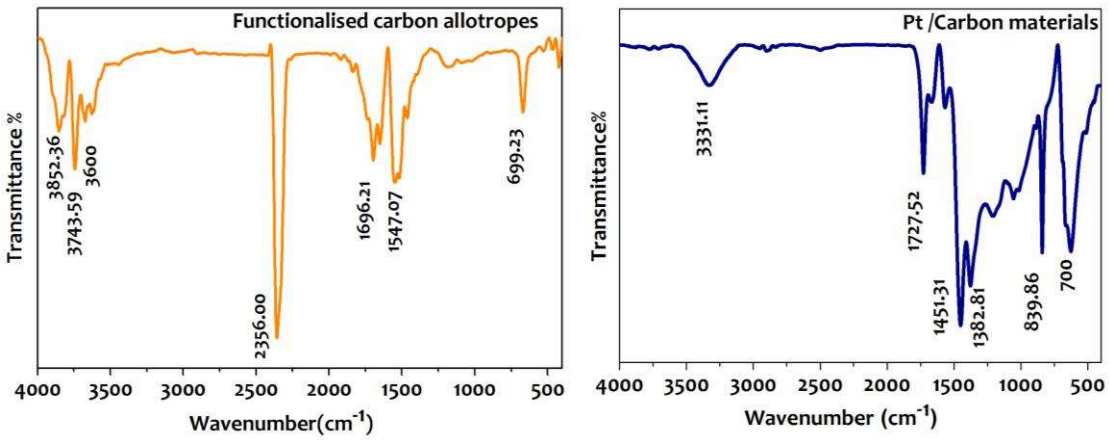

Figure 3.23 FTIR spectra of (a) Functionalised carbon materials, and (b) Pt loaded carbon materials

(b) Pt Loaded Chiral Polyamide

To validate the hypothesis that chiral polyamide interacts with Pt NPs, FTIR spectrometry measurements were conducted on camphoric dichloride, polyamide and Pt loaded polyamide (Figure 3.24). All the samples were prepared in KBr pellets and significant changes in a functional group of composites were observed in the FTIR spectra. Characteristic vibration frequency peaks of polyamide were observed at 3450 (N-H stretching), 2938 (CH_2 stretching), 1652 (C = O stretching), 1548 (N-H bending vibration) and 629 cm^{-1} (N-H bending vibration). The vibration of the N–H groups in polyamide indicated conversion of carbonyl chloride to amide (Figure 3.24b). The presence of Pt on the surface of the polyamide slightly shifted the vibration frequency of the amide group. As shown in Figure 3.24c, N-H and C-N stretching frequencies were raised by 10-20 cm^{-1}, and C=O stretching and N-H bending lowered about 10-50 cm^{-1}. The Pt–O and Pt–N stretching vibrations in the complex gave rise to the characteristic weak peaks at 446 and 532 cm^{-1}. These variations indicated an interactive participation of Pt with polyamide.

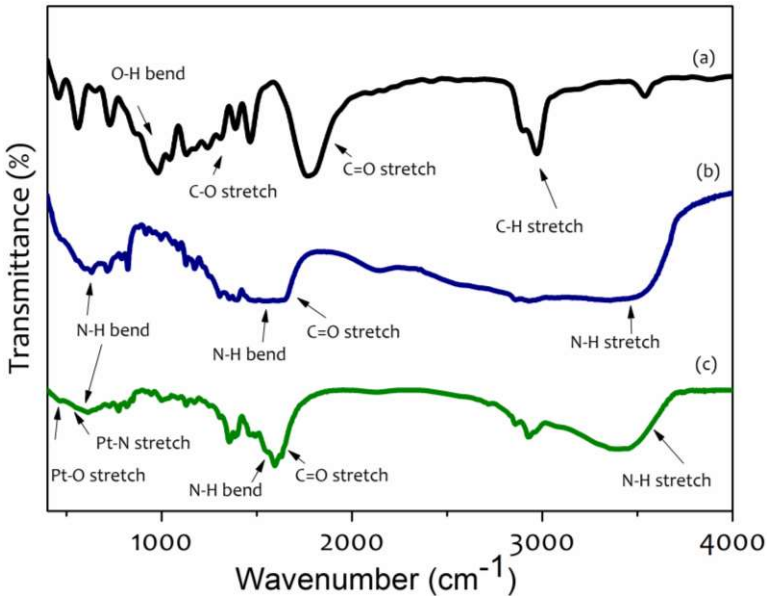

Figure 3.24 FTIR spectra of (a) Chiral camphoric dichloride, (b) Chiral polyamide, and (C) Pt loaded chiral polyamide

3.3.7 Textural characterization of Catalysts

The surface area of Pt loaded carbon materials was determined by adsorption of nitrogen at -196°C. The BET surface area was determined by the BET equation and the (Figure 3.25) pore size distribution was determined from the using the Barrett-Joyner-Halenda (BJH). Before the analysis, samples were degassed under N_2 at 150˚C for 2 h. It was found that carbon materials show high surface area before loading of Pt. After loading of Pt, the surface area of carbon materials decreased. The reduction of the surface area can be explained by clustering of support particles during drying. It is also possible that some of the reduction was caused by the blockage of microspores by Pt or support particles, reducing their availability to N_2 molecules. BJH pore size distribution similar for all catalysts. Out of the various carbon materials, Pt/AC has the highest BET surface area. Surface area and pore size distribution of catalysts (Pt/C) are displayed tabulated in Table 3.6.

Table 3.6 surface areas and BJH pore size distribution of carbon materials and Pt loaded carbon catalysts

S. No.	Catalysts	BET Surface area (m^2/g)	Average Pore size distribution (Å)
1	AC	470.2	17.03
2	Pt/AC	417.0	16.99
3	MWCNT	249.8	17.01
4	Pt/MWCNT	206.3	17.05
5	Graphene	228.4	17.00
6	Pt/Graphene	196.4	17.04
7	CF	141.4	16.95
8	Pt/CF	120.1	16.57

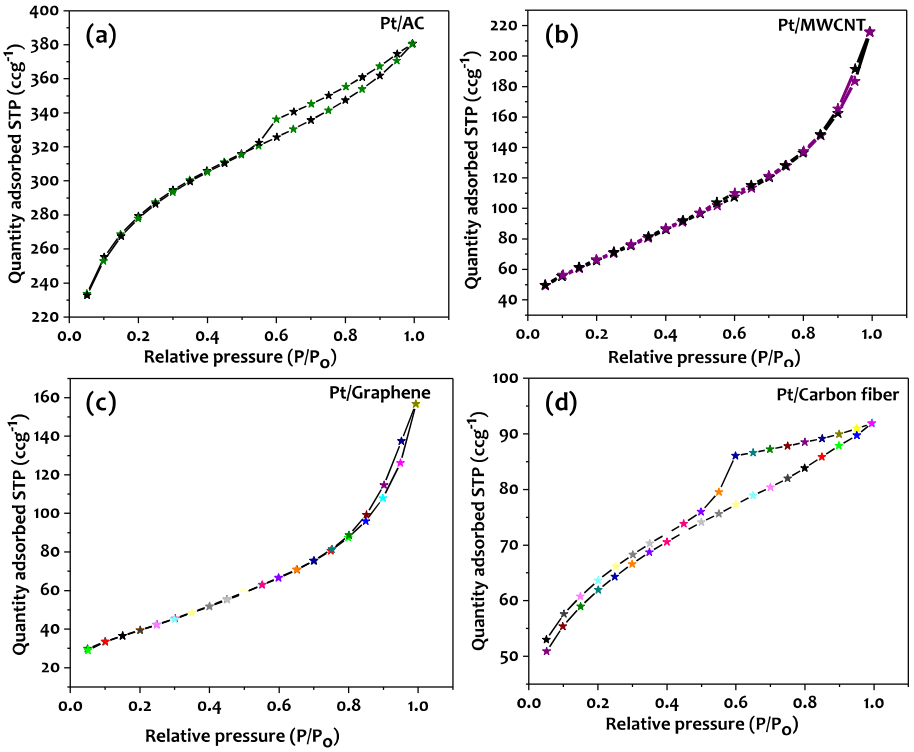

Figure 3.25 BET adsorption-desorption isotherms of (a) Pt/AC, (b) Pt/MWCNT, (C) Pt/Graphene, and (d) Pt/CF

3.4.8 UV Analysis of Catalysts

UV-DRS spectra of MWCNT, Pt/MWCNT, Pt/Cinchonidine/MWCNT, cinchonidine, cinchonine, Pt/Graphene and Pt/CF are shown in Figure 3.26. As observed, cinchonidine produces a steep absorption edge at about 350 nm with poor absorption. Whereas, Pt/MWNTs shows a sharp absorption edge at 375 nm with enhanced absorption in a visible region at 608 nm and 669 nm due to localized surface plasmon resonance (LSPR) associated with platinum nanoparticles. In the presence of cinchonidine, the UV-DRS spectrum of Pt/MWCNTs/Cinchonidine shows reduced absorption due to the bonding of Pt nanoparticles with cinchonidine. Pt/MWCNTs and MWCNTs are observed to exhibit high absorption among all three Pt/C composites.

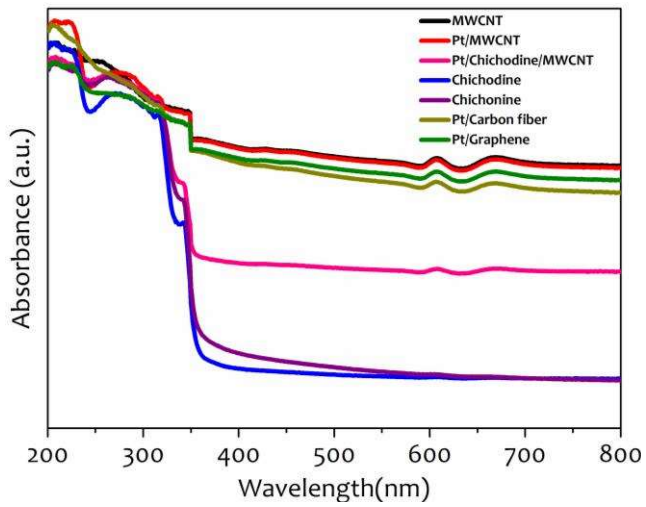

Figure 3.26 DRS of MWCNT, Pt/MWCNT, Pt/Cinchonidine/MWCNT, Cinchonidine, Cinchonine, Pt/Graphene and Pt/CF

3.4.9 TGA Analysis of Catalysts

TGA analyses were carried out for carbon materials and Pt loaded carbon materials (Figure 3.27). The oxidised behaviour of compounds was studied up to 900 °C under N_2. Weight loss below 400 °C is due to desorption of moisture and volatile impurities and, at higher temperature, the carbon material loses most of its starting weight (around 610°C), which increases gradually with the increasing temperature of the post-carbonization. The thermal behaviour of Pt/C showed two main mass loss regions, an initial weight loss around 200-375 °C, corresponding to the desorption of structural H_2O, CO_2 and Pt, and the second peak at ~650 °C, as a result of oxidative decomposition of the carbonaceous materials. Figure 3.27a shows the oxidation behaviour of activated carbon and Pt loaded activated carbon. In activated carbon, in initial first 20 wt % loss occurred before 400 °C and the second 40 to 50 wt % loss in the temperature range of 400-750 °C, due to inorganic impurities and carbon oxidation. Pt/AC catalyst loses 50 wt % at 84 °C and further 10 wt % is lost between 100-800 °C. The weight % loss at low temperature indicates the high surface area of activated carbon with maximum Pt loading. MWCNTs lose 10 wt% before 400°C and the remaining 30 wt% in the temperature of 400-900 °C, whereas for Pt/MWCNT, three regions of weight loss are shown in Figure 3.27b. The first region is due to moisture and in second to inorganic impurities like Pt, and the third carbon oxidation. Graphene shows more stability, only loosing 10 wt% at 800 °C (Figure 3.27c). Pt/graphene shows similar result compare to Pt/MWCNT. Before 400 °C, Pt/graphene oxidised 10 wt%, further 10 wt% was lost before 650 °C and finally graphitised carbon oxidised after 700°C. An interesting result was found for carbon fibers (Figure 3.27d). They lost only 4 wt% until 900 °C. But after loading of Pt, the catalyst started to decompose early. The TGA data confirmed that Pt is successfully coated onto carbon materials. Sometimes during the air oxidation, Pt start to oxidize and present a slightly weight increasing jump in TGA curve. This phenomenon was happened in case of Pt/MWCNT and Pt/CF after 200 °C.

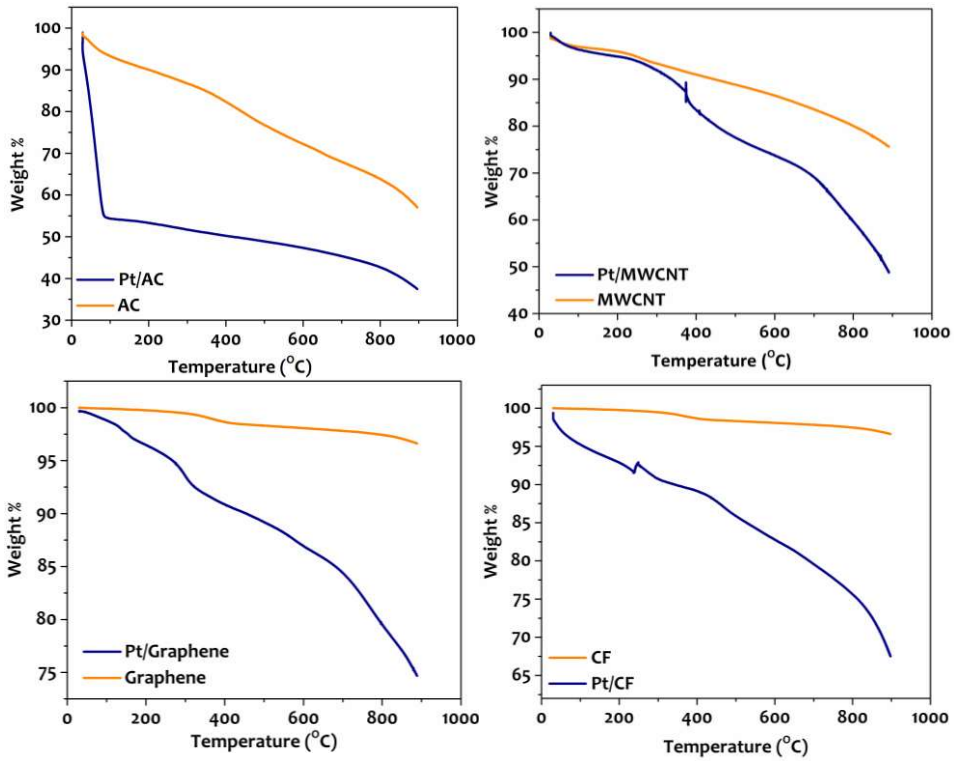

Figure 3.27 TGA analyses of (a) AC and Pt/AC, (b) MWCNT and Pt/MWCNT, (c) Graphene and Pt/Graphene, and (d) CF & Pt/CF

3.4.10 Raman Spectroscopy of Catalysts

Pt loaded carbon materials were investigated by Raman spectroscopy operated at laser excitation wavelength (532 nm, Power source 12.5 mW). Pt and functionalisation defects in carbon materials were examined by Raman spectroscopy (Figure 3.28). The first order Raman allowed G band originating from the stretching of the C-C bond and is common for all sp^2 carbon materials. This band was observed in 1573-1582 cm^{-1} range and is associated with the degree of graphitization in carbon.

After functionalisation of carbon materials, the second band was also obtained at 1360 cm^{-1} (D-band) indicating defects (edges, vacancies and dopants defects) in a graphitic structure of carbon materials [McEvoy *et al,* 2012]. The maximum of the D band was observed in the 1319-1330 cm^{-1} range. The position of this band is dependent of the type of laser used and moves to lower Raman shift with increasing laser wavelength [Wang *et al,* 1990, Ferrari and Robertson 2001, Soin *et al,* 2010]. Choi *et al.* [Choi *et al,* 2013] and Valloerot et al. [Vallerot *et al,* 2006] have reported a D band in the range of 1330- 1350 cm^{-1} and G band in the range of 1579-1582 for MWCNTs at 633 nm. The values of a G-band and D-band for Pt/AC, Pt/MWCNT, Pt/Graphene and Pt/CF are tabulated in Table 3.7. The results obtained from Raman analysis confirmed the functionalisation of carbon materials with Pt.

Table 3.7 Raman results of Pt/carbon materials

Catalysts	G-band	D-band
Pt/AC	1603.5	1350.3
Pt/MWCNT	1575.3	1343.1
Pt/Graphene	1579.5	1350.3
Pt/CF	1589.4	1343.1

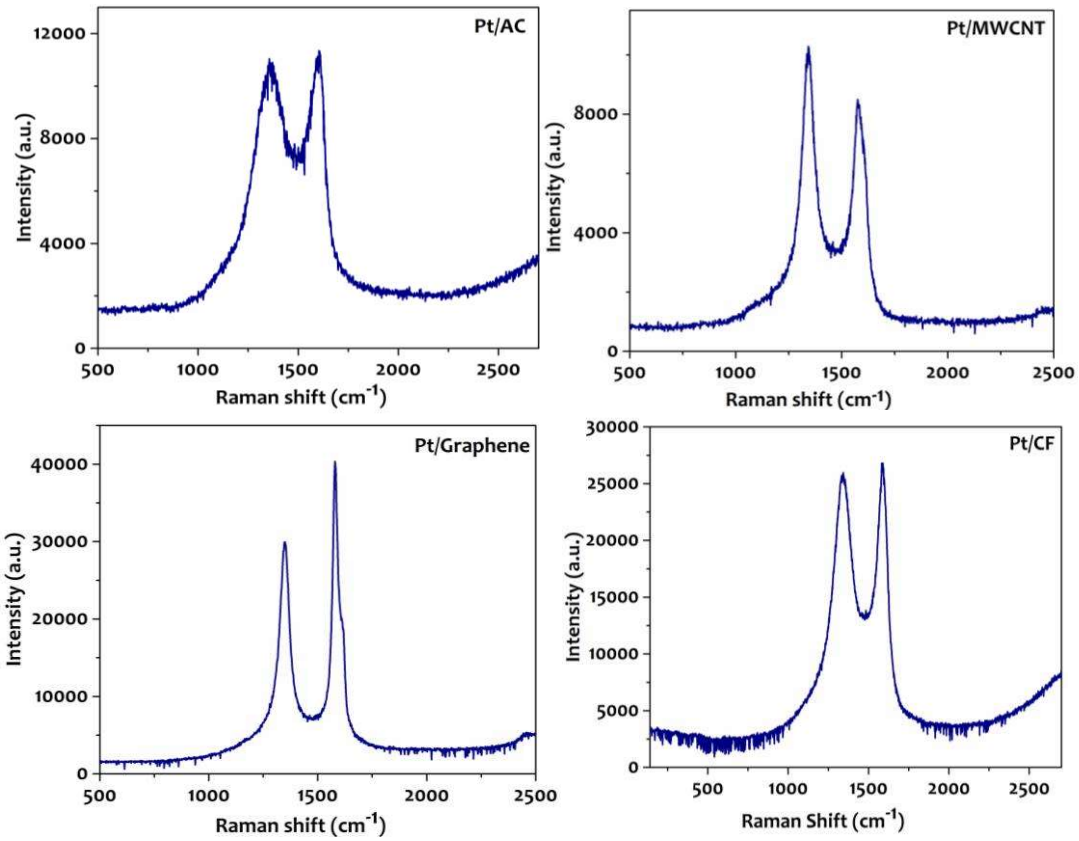

Figure 3.28 Raman spectra of (a) Pt/AC, (b) Pt/MWCNT, (c) Pt/Graphene, and (d) Pt/CF

3.4.11 NMR Analysis

F19 NMR Analysis of F-CD-BF_4

Fluorinated cinchonidine (F-CD-BF_4) was characterized by ^{19}FNMR spectroscopy. ^{19}F NMR spectroscopy was carried out for Selectfluor and fluorinated cinchonidine. In ^{19}F NMR, Selectfluor electrophilic fluorine $[N\text{-}F]^+$ showed a peak at 47.7 ppm, whereas it was shifted at 40.8 ppm in F-CD-BF_4, indicating the transfer of fluorine from Selectfluor to cinchonidine (Figure 3.29). There is no change in BF_4 fluorine peak (at -150 ppm).

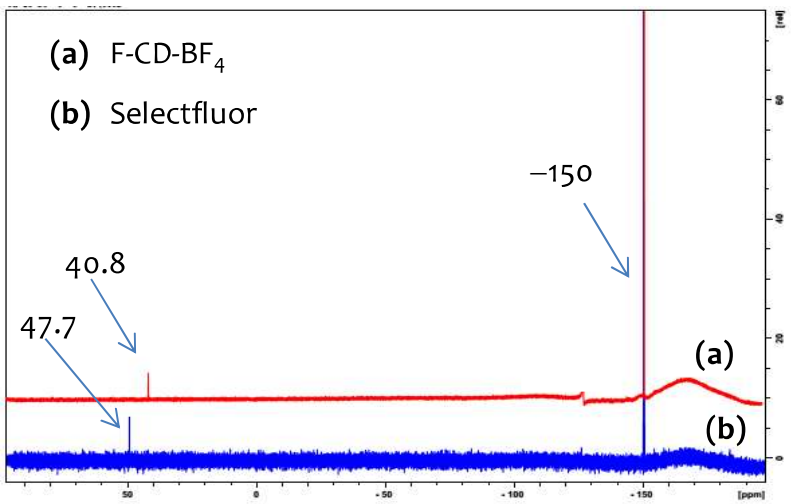

Figure 3.29 F19 NMR spectra of (a) F-CD-BF_4, and (b) Selectfluor

3.4.12 Optical Activity Measurements

CD-UV Analysis

CD spectra were measured at 20°C with 20 nm min^{-1} sweep rate and between 350 and 200 nm. The solvent and cell contribution were subtracted and signals were smoothen. The optical activities of D-camphoric acid and chiral camphoric dichloride are shown in Figure 3.30a, having intense cotton effect with conformational changes. After the irradiation with CPL (circularly polarized light), the 215 nm peak with positive cotton effect for D-camphoric acid ($n \rightarrow \pi^*$ transition of carboxyl group) converted to negative for L-camphoric dichloride, that is maintained after polymerization and metal loading. The negative cotton effect of Poly 5 in 220-240 nm region, suggests the retention in configuration with a helical structure. In UV-Vis spectra (Figure 3.30b), poly 5 shows an absorption peak in the region of 220-240 nm similar to the CD spectra. Comparable observations of catalyst V in CD and UV spectra indicate that the metal incorporation does not alter the stereochemistry of the support and maintains helical structure.

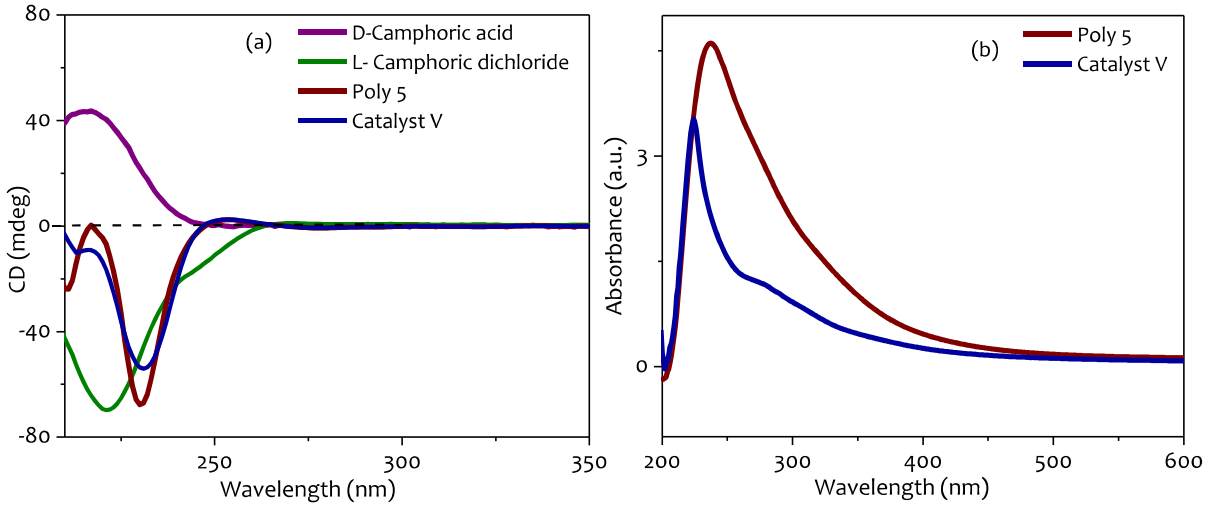

Figure 3.30 (a) CD spectra of D-camphoric acid, L-camphoric dichloride, poly 5 and catalyst V, and (b) UV-Vis spectra of poly 5 and catalyst V

3.4.13 GPC Analysis of Chiral Polyamide

Traditional gel permeation chromatography (GPC) assay was performed to analyze the poly 5 using G2000PW, G3000PW, G4000PW columns. The GPC chromatogram for chiral polyamide is shown in Figure 3.31. The M_n of poly 5 used in catalyst V (15e) is 5.6×10^3 g/mol. The eluent was a 0.2 M solution of $NaNO_3$, circulating with a flow rate of 1.0 mL/min at 25°C, and the sample concentration was approximately 2.5 mg/mL.

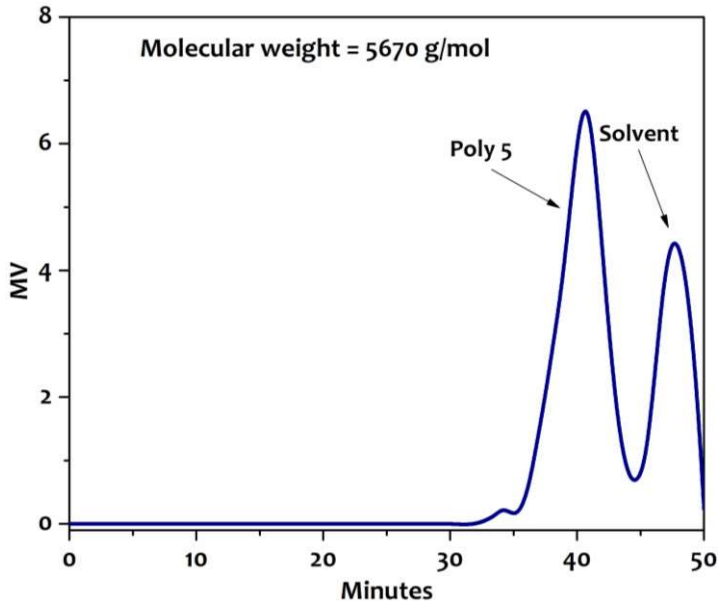

Figure 3.31 GPC chromatogram of poly 5

3.5 CONCLUSION

Metal supported catalysts were prepared and characterized by different analytical techniques. Carbon materials and polymers have remarkable properties favoring their use as supports in heterogeneous catalysis. Out of various supports, carbon nanotubes, graphene, carbon fiber, polyamide and activated carbon were selected as supports. Firstly, Pt loaded carbon materials were prepared using modified wet impregnation method. All the characterization of catalysts confirmed that the metal nanoparticles were successfully attached on the carbon surface. High surface area and porosity of carbon materials were helpful in the dispersion of metal nanoparticles. In this series, Pt hexagonal nanocrystals were prepared using Tween 20 and further loaded on carbon materials. These Pt HNC loaded carbon catalysts were confirmed by different analytical techniques. Secondly, the polymers were found to be a potential candidate for supporting materials. Thus, Pt loaded chiral polyamide (Catalysts l-IV) were prepared and characterized. Chiral polyamide is synthesized by the condensation reaction using chiral and achiral monomers unit. Polyamide supported catalysts were characterized by different analytical techniques and confirmed the attachment of Pt with polyamide. The helical structure of chiral polyamide was confirmed by CD-UV spectroscopy. In the third study, a fluorinated cinchonidine (F-CD-BF_4) was synthesized from fluorinating agents and further loaded on metal loaded carbon nanotubes. The formation of F-CD-BF_4 was confirmed by NMR spectroscopy.